Four-derivative corrections to the neutral-scalar Christodoulou threshold in charged de Sitter black holes

Reggie C. Pantig[1†]

Physics Department, School of Foundational Studies and Education, Mapúa University, 658 Muralla St., Intramuros, Manila 1002, Philippines

Abstract: We study the leading parity-even four-derivative corrections to the linear Christodoulou regularity criterion for a neutral, massless, minimally coupled spectator scalar in four-dimensional charged de Sitter black holes. Within Einstein-Maxwell effective theory, we derive the corrected static solution, cold extremality relation, near-horizon geometry, Cauchy-horizon surface gravity, and neutral scalar quasinormal spectrum. Near cold extremality, the scalar equation analytically reduces to the finite-temperature two-dimensional anti-de Sitter throat problem. We find that the dominant nonstationary spherically symmetric mode retains its cold-limit regularity ratio through first order, whereas higher angular sectors respond to the deformation of the relative throat radii. Nevertheless, the finite-distance neutral-scalar Christodoulou boundary shifts because the relevant exterior scalar spectrum and unequal horizon surface gravities enter the regularity ratio. At small and intermediate cosmological scales, positive effective coefficients move the Christodoulou threshold to larger normalized separations between the Cauchy and event horizons. Along the large-cosmological-scale portion of the cold branch, the same coefficient directions instead move the threshold back toward the cold endpoint. This reversal accompanies a transition in the quasinormal family that determines the spectral gap. We further show that the coefficient combination governing the fixed-charge extremal mass parameter generally differs from those governing the cold throat and the finite-distance neutral-scalar boundary. Extremality therefore does not determine a universal direction for the neutral-scalar Christodoulou-threshold correction. Our results identify the cosmological scale and competition between spectral families as essential elements in relating effective gravity, black-hole extremality, and Cauchy-horizon regularity in this spectator sector.

Keywords: strong cosmic censorship, charged de Sitter black holes, Einstein-Maxwell effective theory, higher-derivative gravity, quasinormal modes, blackhole extremality

DOI: **CSTR:**

CPC Accepted

I. INTRODUCTION

General relativity ties predictability to maximal globally hyperbolic evolution, while charged and rotating black holes reveal the obstruction posed by Cauchy horizons [1, 2]. The classical blueshift picture led to mass inflation and weak null singularities [3, 4]. Subsequent work showed that the outcome depends on the decay entering the interior and on the regularity class used for inextendibility [5−8]. Rigorous analyses further established that a field may remain continuous at the Cauchy horizon while its transverse derivatives lack the regularity required by stronger formulations of strong cosmic censorship [9−13]. We therefore formulate the problem in terms of regularity rather than mere coordinate extendibility.

A positive cosmological constant sharpens this question because exterior perturbations decay exponentially and can compete directly with the exponential blueshift at the inner horizon [5, 6, 14, 15]. Microlocal and nonlinear results place this competition on a precise footing in de Sitter black-hole spacetimes [16−18]. For Reissner-Nordström-de Sitter black holes, quasinormal decay can become sufficiently rapid near extremality to challenge Christodoulou inextendibility [19]. The conclusion depends on the perturbing sector and its regularity [20−22]. In the neutral scalar sector studied here, the relevant quantity is the ratio of the exterior spectral gap to the Cauchy-horizon surface gravity, with the Christodoulou threshold at one half. We restrict every threshold statement below to a neutral, massless, minimally coupled spectator scalar on the corrected background. These statements do not establish the corresponding result for the coupled gravito-electromagnetic system or for nonlinear strong cosmic censorship.

The scalar problem already exhibits nontrivial spectral competition [23]. Charged scalars, superradiance, nonlinear evolution, and quantum stress tensors intro-

Received 23 August 2026; Accepted 23 October 2026

† E-mail: E-mail: rcpantig@mapua.edu.ph

©2026 Chinese Physical Society and the Institute of High Energy Physics of the Chinese Academy of Sciences and the Institute of Modern Physics of the Chinese Academy of Sciences and IOP Publishing Ltd. All rights, including for text and data mining, AI training, and similar technologies, are reserved.

duce additional effects [24−28]. Nonlinear electromagnetic theories provide especially close comparisons. Neutral-scalar strong-cosmic-censorship analyses have been carried out for Born-Infeld-de Sitter, Euler-Heisenberg-de Sitter, and Einstein-Power-Maxwell-de Sitter black holes [29−31]. Related studies in higher dimensions, nonminimal and derivative scalar couplings, and higher-curvature gravity likewise show that the near-extremal regularity region depends on both the theory and the perturbing sector [32−37]. These results show that changes in the charged de Sitter background can alter the regularity threshold and the family that supplies the slowest decay.

Near extremality introduces an additional infrared scale. Extremal Reissner-Nordström black holes already exhibit exceptional scalar behavior [38], while charged de Sitter black holes possess distinct cold, Nariai, and ultracold limits [39, 40]. Nearly extremal quasinormal spectra contain long-lived throat modes, whereas another family is tied to unstable null orbits [41−44]. The least damped family can therefore change as one moves away from the cold limit, making a local throat analysis insufficient for determining the finite-distance neutral-scalar Christodoulou boundary.

Effective field theory provides a common setting for the background, extremality, and spectral corrections. Perturbative field redefinitions reduce the parity-even four-derivative Einstein-Maxwell action to a well-posed basis [45]. Higher-derivative interactions can shift charged-black-hole extremality [46], alter charged-black-hole quasinormal frequencies [47], and enter infrared consistency conditions for photon interactions [48]. These questions also connect to weak-gravity and positivity arguments [49−55]. Their de Sitter interpretation is less universal because different proposals use distinct physical inputs [56−58]. A direct comparison between weak-gravity reasoning and strong cosmic censorship has also been made for a charged scalar on the uncorrected de Sitter black-hole geometry [59].

The specific question we address is narrower than whether higher-order interactions can alter the Christodoulou threshold. Four-dimensional nonlinear-electromagnetic de Sitter backgrounds have already been studied in the Born-Infeld, Euler-Heisenberg, and Einstein-Power-Maxwell cases [29−31], while higher-curvature studies have considered Horndeski and Einstein-Maxwell-Gauss-Bonnet settings [34−36]. In parallel, four-dimensional Einstein-Maxwell effective-theory work has developed reduced operator bases, extremality and positivity relations, and corrected Reissner-Nordström quasinormal spectra [45−48, 50, 51]. De Sitter weak-gravity studies use different physical inputs, including charged-particle bounds and scalar propagation on the two-derivative geometry [56, 58, 59]. The comparison relevant here is between the corrected cold branch, the intrinsic $AdS_2 \times S^2$ throat, the Cauchy-horizon surface gravity, and the full neutral-scalar spectral infimum when all are generated by the same reduced four-derivative coefficients. We carry out this comparison and determine whether the coefficient direction selected by fixed-charge extremality also determines the direction of the finite-distance Christodoulou-threshold shift.

The regularity ratio can respond to the four-derivative terms through two distinct physical effects. The Cauchy-horizon surface gravity fixes the blueshift scale in the denominator, while the least damped exterior scalar mode fixes the decay scale in the numerator. The corrected geometry changes both quantities, and the exterior contribution can change its physical origin when a different quasinormal family supplies the spectral infimum. Unlike comparisons that alter the spacetime theory or perturbing sector separately, our calculation follows one reduced four-dimensional Einstein-Maxwell effective theory through both sides of this ratio. The principal comparison is therefore between the coefficient direction selected by fixed-charge extremality and the branch-dependent direction selected by the finite-distance neutral-scalar threshold.

We work with a purely electric static background and a neutral massless spectator scalar. We derive the corrected black hole, the fixed-charge cold extremality relation, the local throat, the horizon surface gravities, and the finite-distance quasinormal spectrum. This separation allows us to compare the coefficient direction governing the extremal mass parameter, the direction governing the cold throat, and the direction moving the Christodoulou threshold in normalized areal horizon separation. We keep the four-derivative expansion perturbative, exclude the immediate ultracold neighborhood, and interpret the result only as a linear Christodoulou statement for the specified spectator sector. Accordingly, every boundary displacement discussed below refers to this neutral-scalar criterion unless explicitly stated otherwise. Section 2 develops the four-derivative charged de Sitter geometry, including cold extremality and the Cauchy horizon. Section 3 develops the neutral-scalar problem and its cold-limit spectrum. Section 4 treats the full exterior spectrum and mode-family competition. Section 5 determines and interprets the neutral-scalar Christodoulou boundary and its coefficient-space response, Section 6 states the validity and scope, and Section 7 concludes.

II. FOUR-DERIVATIVE CHARGED DE SITTER GEOMETRY

A. Einstein-Maxwell effective theory

We formulate the gravitational theory as a perturbative effective theory about four-dimensional Einstein-Maxwell gravity with a positive cosmological constant.

CPC Accepted

We retain parity-even local interactions with four derivatives and work only to first order in their coefficients. Perturbative field redefinitions allow us to remove operators that differ by the leading equations of motion, integrations by parts, and the four-dimensional Gauss-Bonnet density. Following the reduced four-derivative Einstein-Maxwell basis of Ref. [45], a convenient action is

$$S = \frac{1}{16\pi G}\int d^4x\,\sqrt{-g}\left[R-2\Lambda-\frac{1}{4}X+\varepsilon\left(c_1X^2+c_2Y^2+c_3\mathcal{H}\right)\right], \tag{1}$$

where

$$X=F_{\mu\nu}F^{\mu\nu}, \qquad Y=F_{\mu\nu}\widetilde{F}^{\mu\nu}, \qquad \mathcal{H}=R_{\mu\nu\rho\sigma}\widetilde{F}^{\mu\nu}\widetilde{F}^{\rho\sigma}. \tag{2}$$

We adopt the metric signature $(-+++)$ and define

$$\widetilde{F}^{\mu\nu}=\frac{1}{2}\epsilon^{\mu\nu\rho\sigma}F_{\rho\sigma}. \tag{3}$$

The parameter ε is dimensionless and serves only to track orders in the four-derivative expansion. We set $\varepsilon=1$ only after all expressions have been consistently truncated at first order. The coefficients c_i have dimensions of length squared. Perturbative validity therefore requires $|c_i|/L_{\rm loc}^2 \ll 1$ for each local curvature length $L_{\rm loc}$ relevant to the solution.

The reduced basis in Eq. (1) is sufficient for the present problem. Terms involving R^2, $R_{\mu\nu}R^{\mu\nu}$, RF^2, $R_{\mu\nu}F^{\mu\rho}F^{\nu}{}_{\rho}$, and derivatives of the Maxwell equations can be shifted into the operators in Eq. (1), lower-derivative couplings, or the Gauss-Bonnet density at first perturbative order. We therefore regard G, Λ, and the Maxwell normalization in Eq. (1) as the renormalized two-derivative parameters. We define the electric charge by the conserved flux associated with this normalization.

Equation (1) also fixes the field variables used throughout the paper. In this reduced basis, c_1 multiplies the quartic Maxwell interaction X^2, whereas c_3 multiplies the curvature-Maxwell interaction $\mathcal{H}$. We use these coefficients as coordinates on the chosen operator basis rather than as separately field-redefinition-invariant observables. The neutral spectator scalar is defined in the same field frame by minimal coupling to the metric that appears in Eq. (1). If we perform a further local field redefinition while describing the same theory, the scalar action must be transformed together with the gravitational and electromagnetic variables. Imposing minimal scalar coupling after changing only the gravitational variables would instead specify a different spectator theory. Our frequency shifts and Christodoulou-threshold shifts therefore refer to the reduced action and scalar coupling stated here.

1. *Static spherical reduction*

We seek static, electrically charged solutions in areal-radius coordinates,

$$ds^2=-e^{2\psi(r)}f(r)\,dt^2+\frac{dr^2}{f(r)}+r^2d\Omega_2^2, \qquad F_{tr}=E(r). \tag{4}$$

Spherical symmetry and the absence of magnetic charge imply

$$Y=0. \tag{5}$$

The coefficient c_2 is therefore absent from the background equations. This absence is stronger than the vanishing of Y itself. Because the first variation of Y^2 also vanishes around a purely electric background, c_2 does not modify the static geometry at first order. It can reappear once electromagnetic perturbations are included. Thus, the purely electric background distinguishes the c_1 and c_3 directions in the chosen reduced basis, whereas c_2 remains inactive in the static geometry at this order. This statement does not imply that c_2 is absent from the full effective theory. Perturbations involving electromagnetic degrees of freedom can probe it directly.

For the ansatz in Eq. (4), the remaining invariants reduce to

$$X=-2e^{-2\psi}E^2, \tag{6}$$

and

$$\mathcal{H}=\frac{4(1-f)e^{-2\psi}E^2}{r^2}. \tag{7}$$

After integrating over the angular coordinates and discarding radial total-derivative terms, we obtain the one-dimensional action.

$$L_{\rm red}=2e^{\psi}\left(1-f-rf'-\Lambda r^2\right)+\frac{r^2}{2}e^{-\psi}E^2 +\varepsilon\left[4c_1r^2e^{-3\psi}E^4+4c_3(1-f)e^{-\psi}E^2\right]. \tag{8}$$

The radial form in Eq. (8) makes the perturbative problem particularly simple. The metric equation obtained by varying f contains only the first derivative of ψ, whereas the Maxwell equation can be integrated once because the action depends on the gauge potential only through E.

CPC Accepted

Variation with respect to f gives

$$\psi' = \frac{2\varepsilon c_3}{r} e^{-2\psi} E^2. \tag{9}$$

The integrated Maxwell equation defines the conserved charge Q.

$$Q = r^2 e^{-\psi} E + \varepsilon \left[16 c_1 r^2 e^{-3\psi} E^3 + 8 c_3 (1-f) e^{-\psi} E \right]. \tag{10}$$

The remaining independent metric equation is obtained by variation with respect to ψ,

$$\begin{aligned} 0 = {} & 2e^{\psi} \left(1 - f - r f' - \Lambda r^2\right) - \frac{r^2}{2} e^{-\psi} E^2 \\ & + \varepsilon \left[-12 c_1 r^2 e^{-3\psi} E^4 - 4 c_3 (1-f) e^{-\psi} E^2 \right]. \end{aligned} \tag{11}$$

Thus, only three radial functions remain, and Eqs. (9)–(11) determine them completely once the mass and electric charge are specified.

2. *Perturbative charged de Sitter solution*

We expand the fields about the two-derivative geometry,

$$\begin{aligned} f &= f_0 + \varepsilon f_1 + O(\varepsilon^2), \\ \psi &= \varepsilon \psi_1 + O(\varepsilon^2), \\ E &= E_0 + \varepsilon E_1 + O(\varepsilon^2). \end{aligned} \tag{12}$$

At leading order, Eqs. (9)–(11) reproduce the standard Reissner–Nordström–de Sitter family in our normalization of the electric charge [39].

$$f_0(r) = 1 - \frac{2M}{r} + \frac{Q^2}{4r^2} - \frac{\Lambda r^2}{3}, \qquad E_0(r) = \frac{Q}{r^2}. \tag{13}$$

The normalization of Q follows directly from the coefficient $-X/4$ in Eq. (1). We maintain this convention throughout, so that each correction refers to a single conserved electric flux.

At first order, Eq. (9) can be integrated directly. We choose the additive constant in ψ_1 so that the time coordinate retains its two-derivative normalization. The result is

$$\psi_1(r) = -\frac{c_3 Q^2}{2r^4}. \tag{14}$$

The X^2 interaction does not enter Eq. (14). Thus, the nontrivial lapse arises entirely from the curvature–Maxwell interaction $c_3\mathcal{H}$. This observation also explains why imposing $g_{tt}g_{rr} = -1$ before variation would eliminate a genuine first-order effect.

Expanding the conserved flux relation then yields

$$E_1(r) = -\frac{Q}{6r^6} \left[96 c_1 Q^2 + c_3 \left(-9Q^2 + 96Mr + 16\Lambda r^4 \right) \right]. \tag{15}$$

The electric field contains contributions from both independent coefficients. The c_1 term arises directly from the nonlinear Maxwell interaction, whereas the c_3 term also depends on the gravitational background through M and Λ.

Substituting this result into the remaining metric equation yields

$$f_1(r) = -\frac{c_3 M Q^2}{r^5} - \frac{2 c_3 \Lambda Q^2}{3r^2} - \frac{(4c_1 - c_3) Q^4}{10 r^6}. \tag{16}$$

We choose the integration constant in Eq. (16) such that no additional $1/r$ term appears. Such a term would only redefine M at first order. Similarly, we do not introduce additional terms proportional to Q^2/r^2 or Λr^2, as they would shift the charge normalization or the cosmological constant already fixed in Eq. (1).

Combining Eqs. (13), (14), and (16), the corrected metric takes the form

$$\begin{aligned} f(r) = {} & 1 - \frac{2M}{r} + \frac{Q^2}{4r^2} - \frac{\Lambda r^2}{3} \\ & - \varepsilon \left[\frac{c_3 M Q^2}{r^5} + \frac{2 c_3 \Lambda Q^2}{3r^2} + \frac{(4c_1 - c_3) Q^4}{10 r^6} \right] + O(\varepsilon^2), \end{aligned} \tag{17}$$

and

$$e^{2\psi(r)} = 1 - \varepsilon \frac{c_3 Q^2}{r^4} + O(\varepsilon^2). \tag{18}$$

Several structural features are already evident. The quartic Maxwell interaction modifies only the radial function f and the electric field, whereas the curvature–Maxwell term also changes the redshift function. A positive Λ introduces an additional $c_3 \Lambda Q^2/r^2$ contribution that has no asymptotically flat counterpart. The two effective coefficients therefore enter the global geometry in inequivalent ways, even before extremality is imposed.

3. *Consistency checks*

Direct substitution of Eqs. (14)–(16) into the three first-order radial equations causes each residual to vanish independently, without requiring any relation among c_1, c_3, M, Q, and Λ. The limits $\varepsilon \to 0$ and $Q \to 0$ recover the two-derivative and uncharged geometries, respectively. The limit $\Lambda \to 0$ also exhibits the expected asymptotic-

CPC Accepted

ally flat falloff, with no additional long-range mass, charge, or time-normalization term. Because c_i have dimensions of length squared, f_1 and ψ_1 are dimensionless, while E_1 has dimensions of inverse length. Thus, the expansion in Eq. (12) is dimensionally consistent.

The important structural point is that c_1 and c_3 remain independent in the static solution. The quartic Maxwell term modifies f and E, whereas the curvature-Maxwell term also modifies the redshift function. Consequently, later observables need not depend on the same linear combination of coefficients.

B. Corrected cold extremality

Cold extremality occurs when the Cauchy and event horizons coalesce at a double root of the corrected radial function. Four-derivative interactions shift this degenerate branch. We denote the corresponding areal radius by r_e and impose

$$f(r_e) = 0, \qquad f'(r_e) = 0. \tag{19}$$

A convenient dimensionless measure of the cosmological scale is

$$z = \Lambda r_e^2. \tag{20}$$

At the two-derivative order, the double-root conditions reproduce the standard cold Reissner-Nordström-de Sitter branch [39].

$$M_0 = r_e\left(1 - \frac{2z}{3}\right), \qquad Q_0^2 = 4r_e^2(1-z). \tag{21}$$

The second derivative with respect to the radial coordinate, evaluated on this branch, is

$$f_0''(r_e) = \frac{2(1-2z)}{r_e^2}. \tag{22}$$

Therefore, the ordinary cold branch satisfies

$$0 \leqslant z < \frac{1}{2}. \tag{23}$$

The endpoint $z = 1/2$ corresponds to the ultracold degenerate limit and requires a separate scaling treatment. Throughout the present expansion, we maintain a finite separation from this endpoint.

1. *First-order extremality curve*

We perturb the mass and squared charge while keeping the physical extremal radius fixed.

$$M_{\rm ext} = M_0 + \varepsilon M_1 + O(\varepsilon^2), \quad Q^2_{\rm ext} = Q_0^2 + \varepsilon Q_1^2 + O(\varepsilon^2). \tag{24}$$

Substitution of the corrected radial function into Eq. (19), followed by expansion to first order, yields two algebraic equations for M_1 and Q_1^2. Solving this system yields

$$Q^2_{\rm ext} = 4r_e^2(1-z) + 32\varepsilon(1-z)[c_3 + 4c_1(1-z)] + O(\varepsilon^2). \tag{25}$$

The corresponding extremal mass parameter is given by

$$M_{\rm ext} = r_e\left(1 - \frac{2z}{3}\right) + \frac{2\varepsilon(1-z)}{5r_e}[32c_1(1-z) + c_3(7-2z)] + O(\varepsilon^2). \tag{26}$$

Eqs. (25) and (26) provide the corrected cold curve in parametric form. They describe how the extremal charge and radial mass parameter vary when the physical horizon radius is used to parameterize the branch.

The two coefficient directions enter differently. The charge–radius relation depends on $c_3 + 4c_1(1-z)$, whereas the mass-parameter–radius relation contains a different linear combination. Therefore, a statement about the fixed-charge shift of the extremal mass parameter requires one additional step.

2. *Extremal mass parameter at fixed electric charge*

We first determine how the extremal mass parameter changes when the conserved electric charge is held fixed. This calculation is intrinsic to the chosen static solution and does not yet impose a de Sitter weak-gravity interpretation. We therefore allow the extremal radius itself to shift,

$$r_e \to r_e + \varepsilon\delta r_e + O(\varepsilon^2), \tag{27}$$

while imposing

$$\delta Q^2_{\rm ext} = 0. \tag{28}$$

Expanding Eq. (25) under this condition yields

$$\delta r_e|_Q = -\frac{4(1-z)}{r_e(1-2z)}[c_3 + 4c_1(1-z)]. \tag{29}$$

The factor $1/(1-2z)$ reflects the increasing sensitivity of the cold radius as the ultracold point is approached.

We then vary Eq. (26) while incorporating the radius

CPC Accepted

shift in Eq. (29). The result simplifies to

$$\delta M_{\rm ext}|_Q = -\frac{2(1-z)}{5r_e}\left[8c_1(1-z)+c_3(3+2z)\right]. \tag{30}$$

It is useful to introduce the following combination of coefficients

$$C_M(z) = 8c_1(1-z)+c_3(3+2z). \tag{31}$$

Thus, the fixed-charge mass-parameter shift has the compact form

$$\delta M_{\rm ext}|_Q = -\frac{2(1-z)}{5r_e}C_M(z). \tag{32}$$

Because $1-z>0$ throughout the cold branch, the sign is determined solely by C_M. In our convention,

$$C_M > 0 \tag{33}$$

decreases the extremal mass parameter at fixed charge.

This clarifies what the extremality calculation measures. The form C_M describes a displacement among degenerate solutions at fixed electric flux and contains no information about exterior decay rates or Cauchy-horizon regularity.

We emphasize the interpretation of this quantity. The symbol M denotes the coefficient of the $1/r$ term in the static radial function in our chosen field variables. For $\Lambda>0$, the spacetime has no asymptotic region in which an ADM mass can be defined. We therefore do not identify Eq. (32) with a unique conserved de Sitter mass. Throughout the finite-Λ analysis, we use the phrase extremal mass parameter for $M_{\rm ext}$ and regard Eq. (32) as its fixed-charge displacement. A weak-gravity interpretation is conditional on an independently specified de Sitter mass prescription whose infrared parameterization is compatible with the M used here. In the asymptotically flat limit, the usual interpretation of the $1/r$ coefficient is recovered.

3. *Extremal near-horizon geometry*

The double root permits an independent local determination of the cold geometry. Following the standard extremal near-horizon variational method of Ref. [60], we employ the direct-product ansatz

$$ds^2 = v_1\left(-\rho^2 d\tau^2+\frac{d\rho^2}{\rho^2}\right)+v_2 d\Omega_2^2, \qquad F_{\rho\tau}=e. \tag{34}$$

Here, v_1 and v_2 denote the squared radii of curvature of the AdS_2 and spherical factors. For this geometry, the scalar curvature and Maxwell invariant reduce to

$$R = -\frac{2}{v_1}+\frac{2}{v_2}, \qquad X = -\frac{2e^2}{v_1^2}. \tag{35}$$

The electric field is supported on the AdS_2 factor, whereas its dual is supported on the spherical factor. The curvature–Maxwell interaction therefore contracts the dual field strength with the curvature of S^2. Direct evaluation gives

$$\mathcal{H} = \frac{4e^2}{v_1^2 v_2}. \tag{36}$$

This expression remains nonzero when the leading asymptotically flat extremal geometry satisfies $v_1=v_2$. Therefore, the local effect of $c_3\mathcal{H}$ does not originate from a difference between the two product radii. Instead, the cosmological constant changes the background ratio v_1/v_2 and the manner in which the first-order deformation approaches the ultracold endpoint.

We divide the angularly integrated Lagrangian by its common factor 4π and omit the overall factor $1/(16\pi G)$. With this normalization, the reduced near-horizon functional is

$$\mathfrak{f} = 2v_1-2v_2-2\Lambda v_1 v_2+\frac{e^2 v_2}{2v_1}+\varepsilon\left[\frac{4c_3e^2}{v_1}+\frac{4c_1e^4v_2}{v_1^3}\right]. \tag{37}$$

The electric variation adopts the same charge normalization as the flux relation in Eq. (10). Extremizing the reduced functional yields

$$\frac{\partial\mathfrak{f}}{\partial v_1}=0, \qquad \frac{\partial\mathfrak{f}}{\partial v_2}=0, \qquad \frac{\partial\mathfrak{f}}{\partial e}=Q. \tag{38}$$

At two-derivative order, the latter relation yields $Q=ev_2/v_1$, in agreement with the conserved electric flux following the near-horizon scaling of the global solution. We parameterize the solution in terms of the physical spherical radius,

$$v_2 = r_e^2. \tag{39}$$

Solving Eq. (38) perturbatively reproduces the extremal charge relation given in Eq. (25). The AdS_2 radius is

$$v_1 = \frac{r_e^2}{1-2z}+\frac{8\varepsilon(1-z)}{(1-2z)^2}\left[c_3+8c_1(1-z)\right]+O(\varepsilon^2). \tag{40}$$

We define the second combination of coefficients

CPC Accepted

$$C_A(z) = c_3 + 8c_1(1-z). \tag{41}$$

Thus, the local throat deformation is governed by C_A, whereas the fixed-charge shift in the extremal mass parameter is governed by C_M. Their difference is

$$C_M(z) - C_A(z) = 2c_3(1+z). \tag{42}$$

No general equality holds between these two combinations. Consequently, the extremal mass parameter and the intrinsic AdS_2 geometry probe inequivalent directions in the two-dimensional coefficient space whenever $c_3 \neq 0$.

4. *Consistency and limiting behavior*

The near-horizon variational equations independently reproduce the extremal charge relation in Eq. (25), while the corrected radial function yields the same AdS_2 radius via $v_1 = 2/f''(r_e)$. Thus, both checks describe the same corrected cold branch. The limit $z \to 0$ is finite for the extremal charge, the fixed-charge mass-parameter shift, and v_1. In particular, the c_3 contribution to the local throat survives in the asymptotically flat extremal limit, consistent with Eq. (36).

The standard cold expansion becomes nonuniform as $z \to 1/2$, because the fractional correction to v_1 is enhanced by $(1-2z)^{-1}$. We exclude this immediate ultracold neighborhood. Away from this region, the fixed-charge mass-parameter shift probes C_M, whereas the intrinsic throat probes C_A. Their difference in Eq. (42) shows that extremality and local throat geometry already define inequivalent directions in coefficient space.

C. Cauchy-horizon geometry

The corrected geometry determines the locations of the three horizons and, in particular, the surface gravity of the Cauchy horizon. This quantity sets the local blueshift scale entering the neutral-scalar Christodoulou regularity test used below. We first treat nondegenerate horizons perturbatively and then use a separate expansion for the cold region, in which the Cauchy and event horizons approach one another.

1. *Displacement of simple horizons*

Let $\bar{r}_a$ denote a simple root of the two-derivative radial function.

$$a \in \{-,+,c\}, \qquad f_0(\bar{r}_a) = 0, \qquad f_0'(\bar{r}_a) \neq 0. \tag{43}$$

We expand the corresponding corrected root as

$$r_a = \bar{r}_a + \varepsilon \delta r_a + O(\varepsilon^2). \tag{44}$$

Expanding the horizon condition $f(r_a) = 0$ yields

$$\delta r_a = -\frac{f_1(\bar{r}_a)}{f_0'(\bar{r}_a)}. \tag{45}$$

This expression applies to the Cauchy, event, and cosmological horizons, provided that the relevant root remains nondegenerate.

For later use, we introduce quantities evaluated at each two-derivative horizon,

$$x_a = \frac{Q^2}{4\bar{r}_a^2}, \qquad z_a = \Lambda \bar{r}_a^2, \qquad \Delta_a = 1 - x_a - z_a. \tag{46}$$

Using the horizon equation to eliminate M, the derivative of the radial function becomes

$$f_0'(\bar{r}_a) = \frac{\Delta_a}{\bar{r}_a}. \tag{47}$$

Substituting the first-order metric correction derived in Section 2 into Eq. (45), we obtain

$$\delta r_a = \frac{2x_a}{5\bar{r}_a \Delta_a}\left[16c_1 x_a + c_3(5 + x_a + 5z_a)\right]. \tag{48}$$

The factor $1/\Delta_a$ indicates the expected limitation of the simple-root expansion. On the cold branch, Δ_- and Δ_+ vanish as the two black-hole horizons merge. Consequently, their individual displacements become nonuniform, even when the four-derivative coefficients remain small.

A sufficient condition for treating the two roots as perturbations of distinct two-derivative horizons is

$$\frac{\varepsilon \max(|c_1|,|c_3|)}{r_e^2} \ll \eta^2, \tag{49}$$

where η quantifies the separation of the cold pair. We do not impose Eq. (49) in the near-cold analysis; instead, we expand directly about the corrected extremal geometry.

2. *Surface gravities of simple horizons*

Using the standard Killing-horizon normalization [2], we define the signed surface gravity for the static Killing field ∂_t by

$$\widehat{\kappa}_a = \frac{1}{2} e^{\psi(r_a)} f'(r_a). \tag{50}$$

The physical surface gravity is

$$\kappa_a = \left|\widehat{\kappa}_a\right|. \tag{51}$$

CPC Accepted

Expanding Eq. (50) about a simple two-derivative root yields

$$\widehat{\kappa}_a = \frac{1}{2} f_0'(\bar{r}_a) + \varepsilon \delta\widehat{\kappa}_a + O(\varepsilon^2), \tag{52}$$

with

$$\delta\widehat{\kappa}_a = \frac{1}{2}\left[\psi_1 f_0' + f_1' - \frac{f_1 f_0''}{f_0'}\right]_{r=\bar{r}_a}. \tag{53}$$

The last term originates from the displacement of the horizon itself. Omitting this term would evaluate the derivative of the corrected metric at an incorrect radial position.

We can express the result compactly by defining

$$\begin{aligned}\mathcal{P}(x,z) &= 16c_1 x(-2+x+3z) \\ &\quad + c_3\left(-5-2x+x^2+10z-2xz+5z^2\right).\end{aligned} \tag{54}$$

Eq. (53) then reduces to

$$\delta\widehat{\kappa}_a = -\frac{2x_a}{5\bar{r}_a^3\Delta_a}\mathcal{P}(x_a, z_a). \tag{55}$$

The signed derivative is negative at the Cauchy horizon. Therefore, we have

$$\kappa_- = -\frac{\Delta_-}{2\bar{r}_-} + \varepsilon\frac{2x_-}{5\bar{r}_-^3\Delta_-}\mathcal{P}(x_-, z_-) + O(\varepsilon^2). \tag{56}$$

Eq. (56) gives the required inner-horizon surface gravity provided that the Cauchy horizon remains a simple root. The cosmological horizon also remains nondegenerate in the standard cold limit and can be treated using the same expression.

The pole in Eq. (55) should not be interpreted as a physical divergence. It indicates that perturbing the locations of two nearly coincident simple roots is not the appropriate expansion near cold extremality.

3. *Near-cold geometry*

For the near-cold region, we expand about the corrected extremal solution derived in Section 2.2 and measure the physical separation between the Cauchy and event horizons as follows:

$$\eta = \frac{r_+ - r_-}{2r_e}, \qquad 0 < \eta \ll 1. \tag{57}$$

To leading order in this separation,

$$r_\pm = r_e(1 \pm \eta) + O(\eta^2). \tag{58}$$

Let

$$\delta = \eta r_e. \tag{59}$$

Near the corrected double root, the radial function assumes the universal quadratic form

$$f(r) = \frac{(r-r_e)^2 - \delta^2}{v_1} + O(\eta^3), \tag{60}$$

where v_1 is the corrected AdS_2 radius obtained from the extremal throat.

The redshift function changes only at higher order across the narrow interval between the two horizons. Its value at the extremal radius is

$$\psi_e = -\frac{2\varepsilon c_3(1-z)}{r_e^2} + O(\varepsilon^2). \tag{61}$$

Equations (60) and (61) show that, to leading order in η, both black hole horizons have the same magnitude of surface gravity,

$$\kappa_+ = \kappa_- = \frac{e^{\psi_e}\delta}{v_1} + O(\eta^2). \tag{62}$$

Substituting the corrected throat radius and expanding yields

$$\begin{aligned}\kappa_- &= \frac{\eta}{r_e}(1-2z) - \frac{2\varepsilon\eta(1-z)}{r_e^3}\left[32c_1(1-z) + c_3(5-2z)\right] \\ &\quad + O(\eta^2) + O(\varepsilon\eta^2) + O(\varepsilon^2\eta).\end{aligned} \tag{63}$$

The same expression holds for κ_+ to the order shown. We independently verified Eq. (63) by expanding $e^{\psi_e}\delta/v_1$. The difference between the direct expansion and the displayed result vanishes identically.

We define the coefficient combination that governs the leading inner-horizon blueshift correction,

$$C_\kappa(z) = 32c_1(1-z) + c_3(5-2z). \tag{64}$$

The near-cold expression can then be written as

$$\kappa_- = \frac{\eta}{r_e}(1-2z) - \frac{2\varepsilon\eta(1-z)}{r_e^3}C_\kappa(z) + O(\eta^2) + O(\varepsilon\eta^2) + O(\varepsilon^2\eta). \tag{65}$$

The dependence on η has a direct geometric origin: at exact cold extremality, the double root has zero surface gravity; therefore, the leading nonzero contribution must be linear in the horizon separation.

CPC Accepted

The direction of the coefficient in Eq. (64) differs from the extremal mass-parameter direction obtained previously. In particular,

$$C_\kappa(z) - C_M(z) = 24c_1(1-z) + 2c_3(1-2z). \tag{66}$$

Therefore, the sign of the fixed-charge extremal mass-parameter shift does not determine the sign of the correction to the Cauchy-horizon surface gravity.

This distinction has an immediate physical meaning. Extremality fixes a relation among the conserved charge, the radial mass parameter, and the degenerate horizon within the chosen static variables. By contrast, κ_- measures the local exponential scale associated with the inner horizon of a nonextremal black hole. Four-derivative interactions need not modify these quantities in the same direction.

The equality of κ_+ and κ_- at leading order in the cold limit will also be important for the neutral scalar spectrum. Their first relative difference enters only beyond the leading term in η. Consequently, the strict cold-limit value of the spectral ratio can exhibit cancellations that are not apparent from the inner-horizon geometry alone.

III. NEUTRAL SCALAR PROBLEM AND COLD-LIMIT SPECTRUM

A. Neutral scalar perturbations

We treat a neutral massless scalar as a spectator field on the corrected charged de Sitter geometry. It therefore probes the four-derivative modification of the spacetime without sourcing additional corrections to the background. This choice isolates the geometric contribution to exterior decay and provides the simplest setting for comparing that decay with the Cauchy-horizon blueshift derived in Section 2.3.

The standard equation for a minimally coupled massless scalar and its separated quasinormal-mode formulation are reviewed, for example, in Ref. [41]. The scalar obeys

$$\Box\Phi_s = 0. \tag{67}$$

Spherical symmetry allows the field to be decomposed as

$$\Phi_s = e^{-i\omega t} Y_{\ell m}(\theta,\phi)\frac{\Psi(r)}{r}, \tag{68}$$

where the spherical harmonics satisfy

$$\nabla^2_{S^2} Y_{\ell m} = -\ell(\ell+1) Y_{\ell m}. \tag{69}$$

The frequency ω is generally complex. Modes with a negative imaginary part decay in the static region between the event and cosmological horizons.

1. *Radial wave equation*

The radial part is simplified by introducing the tortoise coordinate via

$$\frac{dr_*}{dr} = \frac{e^{-\psi(r)}}{f(r)}. \tag{70}$$

The scalar equation then assumes the Schrödinger form

$$\frac{d^2\Psi}{dr_*^2} + \left[\omega^2 - V_\ell(r)\right]\Psi = 0. \tag{71}$$

A direct reduction of the covariant wave operator yields

$$V_\ell(r) = e^{2\psi(r)} f(r)\left[\frac{\ell(\ell+1)}{r^2} + \frac{f'(r) + f(r)\psi'(r)}{r}\right]. \tag{72}$$

Rewriting Eq. (71) in terms of the areal-radius coordinate verifies Eq. (72). The resulting expression exactly reproduces the separated covariant wave equation.

The potential vanishes at each simple horizon because $f(r_a) = 0$. In the static region,

$$r_+ < r < r_c, \tag{73}$$

The quasinormal problem therefore describes scattering between two asymptotically free ends in the tortoise coordinate. The two-derivative potential is obtained immediately as

$$V_\ell^{(0)} = f_0\left[\frac{\ell(\ell+1)}{r^2} + \frac{f_0'}{r}\right]. \tag{74}$$

We expand the corrected potential as

$$V_\ell = V_\ell^{(0)} + \varepsilon\delta V_\ell + O(\varepsilon^2). \tag{75}$$

Using the metric corrections obtained in Section 2, the first-order term becomes

$$\delta V_\ell = (f_1 + 2\psi_1 f_0)\left[\frac{\ell(\ell+1)}{r^2} + \frac{f_0'}{r}\right] + \frac{f_0}{r}\left(f_1' + f_0\psi_1'\right). \tag{76}$$

The compact form in Eq. (76) separates two distinct effects. The first line modifies the overall height and

CPC Accepted

shape inherited from the two-derivative potential. The second line arises from radial variations in the corrected geometry. We retain this form in the spectral calculation because expanding it into individual inverse powers of r would not add physical information.

In the spherically symmetric sector, the angular barrier vanishes, and the potential reduces to

$$V_0(r) = e^{2\psi} f \frac{f' + f\psi'}{r}. \tag{77}$$

This sector becomes especially important near cold extremality because the angular term does not contribute a first-order correction to its leading throat conformal weight.

2. *Quasinormal boundary conditions*

We now impose the standard causal quasinormal-mode boundary conditions for a de Sitter static region [41]. Near a nondegenerate event horizon, the tortoise coordinate behaves as

$$r_* = \frac{1}{2\kappa_+} \ln(r - r_+) + O(1). \tag{78}$$

Regularity at the future event horizon selects the ingoing solution

$$\Psi \sim e^{-i\omega r_*} \sim (r - r_+)^{-i\omega/(2\kappa_+)}. \tag{79}$$

At the cosmological horizon,

$$r_* = -\frac{1}{2\kappa_c} \ln(r_c - r) + O(1), \tag{80}$$

and regularity at the future cosmological horizon selects the outgoing branch

$$\Psi \sim e^{+i\omega r_*} \sim (r_c - r)^{-i\omega/(2\kappa_c)}. \tag{81}$$

The quasinormal frequencies are therefore the discrete complex values of ω for which a single solution of Eq. (71) satisfies Eqs. (79) and (81).

The lapse correction does not alter the form of these boundary conditions. It enters through the corrected surface gravities and through the relation between r and r_*. A constant rescaling of the time coordinate multiplies both ω and each surface gravity by the same factor. Ratios constructed from these quantities are therefore invariant under such a rescaling.

For the numerical work below, it is useful to remove the known singular powers explicitly. We write

$$\Psi(r) = (r - r_+)^{-i\omega/(2\kappa_+)} (r_c - r)^{-i\omega/(2\kappa_c)} y(r), \tag{82}$$

where $y(r)$ is regular on the closed interval bounded by the two outer horizons. This formulation recasts the quasinormal-mode problem as a regular eigenvalue problem suitable for spectral discretization.

3. *Spectral structure and scope*

The frequencies can be written as the perturbative expansion

$$\omega_{n\ell} = \omega_{n\ell}^{(0)} + \varepsilon\delta\omega_{n\ell} + O(\varepsilon^2). \tag{83}$$

The shift depends on the complete exterior geometry and both horizon boundary conditions, rather than only on the local value of δV_ℓ. Near cold extremality, a purely damped family approaches the $AdS_2 \times S^2$ throat spectrum, whereas photon-sphere and de Sitter-type families can become competitive at finite separation. We therefore identify the least-damped nonstationary mode only after comparing the relevant families.

The scalar is neutral, massless, and minimally coupled to the metric variable fixed by Eq. (1). With this choice, c_2 remains absent, and the spectrum probes (c_1, c_3) through the corrected background. Any further change of field variables must be accompanied by the induced change in the scalar action if it is to describe the same spectator theory. This spectator sector isolates the geometric contribution to the regularity ratio but does not determine the spectra of coupled gravitational and electromagnetic perturbations, for which additional coefficient dependence can appear.

B. Analytic cold-limit spectrum

Near the cold-extremal limit, the radial interval between the nearly degenerate black-hole horizons develops a finite-temperature deformation of the extremal $AdS_2 \times S^2$ throat. The equation for a neutral scalar becomes exactly solvable at leading order in the horizon separation. This reduction analytically determines how the four-derivative interactions modify the near-extremal frequencies before we solve the full exterior problem.

We keep the effective expansion to first order in ε and retain the leading nonzero term in the near-cold parameter η. The extremal quantities v_1, v_2, and r_e are those obtained in Section 2.2.

1. *Finite-temperature AdS_2 throat*

Near the corrected double root, the radial function takes the form

$$f(r) = \frac{(r - r_e)^2 - \delta^2}{v_1} + O(\eta^3), \qquad \delta = \eta r_e. \tag{84}$$

CPC Accepted

Across the narrow throat region, the lapse can be replaced, to the order required here, by its extremal value.

$$\psi(r) = \psi_e + O(\eta). \tag{85}$$

We define the dimensionless radial coordinate

$$x = \frac{r - r_e}{\delta}. \tag{86}$$

The two black-hole horizons are then located at $x = -1$ and $x = 1$. Rescaling the time coordinate according to

$$\tau = \kappa_{\rm NH} t, \qquad \kappa_{\rm NH} = \frac{e^{\psi_e}\delta}{v_1}, \tag{87}$$

reduces the leading near-cold metric to

$$ds^2 = v_1\left[-(x^2-1)d\tau^2 + \frac{dx^2}{x^2-1}\right] + v_2 d\Omega_2^2 + O(\eta). \tag{88}$$

The event horizon corresponds to $x = 1$. The region $x > 1$ describes the exterior portion of the throat, which connects to the full de Sitter static region.

The scale $\kappa_{\rm NH}$ agrees with the event- and Cauchy-horizon surface gravities at leading order in the cold limit. Using the corrected extremal geometry, we obtain

$$\kappa_{\rm NH} = \kappa_+ + O(\eta^2) = \kappa_- + O(\eta^2). \tag{89}$$

This equality includes the first-order four-derivative contribution proportional to $\varepsilon\eta$, which causes the leading surface-gravity correction to cancel in the cold-limit ratio β.

2. *Scalar equation on the throat*

We separate the scalar field directly on the geometry given in Eq. (88).

$$\Phi_{\rm s} = e^{-i\widehat{\omega}\tau} Y_{\ell m}(\theta,\phi) R(x), \tag{90}$$

where

$$\widehat{\omega} = \frac{\omega}{\kappa_{\rm NH}}. \tag{91}$$

The finite-temperature AdS_2 scalar problem underlying the near-extremal Reissner-Nordström-de Sitter family is standard [19, 23]. For our corrected throat, the radial equation derived from the covariant wave equation becomes

$$\frac{d}{dx}\left[(x^2-1)\frac{dR}{dx}\right] + \left[\frac{\widehat{\omega}^2}{x^2-1} - \ell(\ell+1)\frac{v_1}{v_2}\right] R = 0. \tag{92}$$

Thus, the angular momentum appears as an effective mass on AdS_2. The ratio v_1/v_2 encodes all four-derivative information that survives in the dimensionless radial equation at the order considered here.

We define ν_ℓ by

$$\nu_\ell(\nu_\ell + 1) = \ell(\ell+1)\frac{v_1}{v_2}. \tag{93}$$

The root associated with the branch that decays toward the outer part of the throat is

$$\nu_\ell = -\frac{1}{2} + \sqrt{\frac{1}{4} + \ell(\ell+1)\frac{v_1}{v_2}}. \tag{94}$$

The radial equation is an associated Legendre equation. A solution exhibiting ingoing behavior at the future event horizon is

$$R_{\rm in}(x) = P_{\nu_\ell}^{i\widehat{\omega}}(x). \tag{95}$$

Eq. (95) satisfies Eq. (92) provided that Eq. (93) is imposed.

Near $x = 1$, the selected branch behaves as

$$R_{\rm in} = C_+ (x-1)^{-i\widehat{\omega}/2}[1 + O(x-1)], \tag{96}$$

which is regular at the future event horizon in ingoing coordinates.

At large x, the same solution separates into growing and decaying power-law terms,

$$R_{\rm in} = A_\ell x^{\nu_\ell} + B_\ell x^{-\nu_\ell - 1} + O\left(x^{-\nu_\ell - 3}\right). \tag{97}$$

The coefficient of the growing branch includes the factor

$$A_\ell \sim \frac{1}{\Gamma\left(\nu_\ell + 1 - i\widehat{\omega}\right)}. \tag{98}$$

For $\ell \geq 1$, near-extremal resonances arise when this coefficient vanishes. The poles of the gamma function require

$$\nu_\ell + 1 - i\widehat{\omega} = -n, \qquad n = 0, 1, 2, \ldots, \qquad \ell \geqslant 1. \tag{99}$$

CPC Accepted

Solving Eq. (99) gives

$$\widehat{\omega}_{n\ell} = -i(n+\nu_\ell+1), \qquad \ell \geqslant 1. \tag{100}$$

We analyze the spherically symmetric sector separately below because the normalization of the associated Legendre solution becomes singular as $\nu_\ell \to 0$.

It is useful to identify the conformal weight of the effective AdS_2 scalar:

$$\Delta_\ell = \frac{1}{2} + \sqrt{\frac{1}{4} + \ell(\ell+1)\frac{v_1}{v_2}}. \tag{101}$$

For $\ell \geqslant 1$, the leading near-extremal frequencies can therefore be written in the compact form

$$\omega_{n\ell}^{\mathrm{NE}} = -i\kappa_{\mathrm{NH}}(n+\Delta_\ell) + O(\eta^2), \qquad \ell \geqslant 1. \tag{102}$$

The absence of a real part at this order reflects the purely damped nature of the throat family. Corrections beyond the leading cold scaling may depend on the exterior geometry and need not preserve the simple form in Eq. (102).

3. *Four-derivative shift of the conformal weight*

The corrected throat geometry modifies the scalar spectrum through the ratio v_1/v_2. Expanding this ratio to first order gives

$$\frac{v_1}{v_2} = \frac{1}{1-2z} + \frac{8\varepsilon(1-z)}{r_e^2(1-2z)^2}C_A(z) + O(\varepsilon^2). \tag{103}$$

We define the positive two-derivative quantity

$$D_\ell(z) = \sqrt{\frac{1}{4} + \frac{\ell(\ell+1)}{1-2z}}. \tag{104}$$

The conformal weight then becomes

$$\Delta_\ell = \frac{1}{2} + D_\ell(z) + \varepsilon\frac{4\ell(\ell+1)(1-z)}{r_e^2(1-2z)^2 D_\ell(z)}C_A(z) + O(\varepsilon^2). \tag{105}$$

Two distinct geometric effects contribute to the dimensionful frequency in Eq. (102). The surface-gravity scale changes through the corrected lapse and AdS_2 radius, whereas the dimensionless conformal weight changes through the ratio of the two throat radii. For $\ell \geqslant 1$, we can therefore write

$$\begin{aligned} -\mathrm{Im}\,\omega_{n\ell}^{\mathrm{NE}} = {} & \kappa_{\mathrm{NH}}^{(0)}\left[n+\Delta_\ell^{(0)}\right] + \varepsilon\delta\kappa_{\mathrm{NH}}\left[n+\Delta_\ell^{(0)}\right] \\ & + \varepsilon\kappa_{\mathrm{NH}}^{(0)}\delta\Delta_\ell + O(\eta^2) + O(\varepsilon^2\eta). \end{aligned} \tag{106}$$

The first correction in Eq. (106) modifies the overall near-horizon timescale. The second modifies the dimensionless spectrum itself. Only the latter survives in the strict cold limit of the ratio relevant to Cauchy-horizon regularity.

4. *Cold-limit spectral ratio*

For a single near-extremal mode, we define

$$\beta_{n\ell}^{\mathrm{NE}} = \frac{-\mathrm{Im}\,\omega_{n\ell}^{\mathrm{NE}}}{\kappa_-}. \tag{107}$$

From Eq. (89), the ratio of the throat scale to the Cauchy-horizon surface gravity is given by

$$\frac{\kappa_{\mathrm{NH}}}{\kappa_-} = 1 + O(\eta). \tag{108}$$

For $\ell \geqslant 1$, the leading-order cold-limit result is therefore

$$\beta_{n\ell}^{\mathrm{NE}} = n + \Delta_\ell + O(\eta), \qquad \ell \geqslant 1. \tag{109}$$

Substitution of Eq. (105) gives

$$\begin{aligned} \beta_{n\ell}^{\mathrm{NE}} = {} & n + \frac{1}{2} + D_\ell(z) + \varepsilon\frac{4\ell(\ell+1)(1-z)}{r_e^2(1-2z)^2 D_\ell(z)}C_A(z) \\ & + O(\eta) + O(\varepsilon\eta) + O(\varepsilon^2), \quad \ell \geqslant 1. \end{aligned} \tag{110}$$

The correction proportional to C_κ is absent from the strictly cold term. Both the quasinormal decay rate and the inner-horizon surface gravity inherit the same leading near-horizon time scale, so this common factor cancels in β.

The remaining correction is entirely geometric. It quantifies how the four-derivative terms modify the relative curvature radii of AdS_2 and S^2.

For every $\ell \geqslant 1$, the prefactor multiplying C_A is positive on the ordinary cold branch. We therefore obtain

$$\mathrm{sgn}\left(\delta\beta_{n\ell}^{\mathrm{NE}}\right) = \mathrm{sgn}\left(C_A(z)\right), \qquad \ell \geqslant 1. \tag{111}$$

The overtone number does not affect the sign at leading order in the cold limit.

5. *Spherically symmetric endpoint and the normalization limit*

The lowest angular-momentum sector requires separate treatment. Setting $\ell = 0$ in Eq. (92) gives $\nu_0 = 0$ and $\Delta_0 = 1$. Direct substitution of $\nu_0 = 0$ into the unnormal-

CPC Accepted

ized associated Legendre solution is insufficient at the fundamental frequency, because the same gamma function that eliminates the large-x branch also appears in the overall normalization. We therefore avoid using this singular normalization in the limiting step.

For auxiliary $\nu > 0$, the fundamental condition in Eq. (99) is $\widehat{\omega} = -i(\nu+1)$. Along this branch, we solve the radial equation directly with

$$\widetilde{R}_\nu(x) = \left(x^2-1\right)^{-(\nu+1)/2}. \tag{112}$$

Direct substitution gives

$$\frac{d}{dx}\left[\left(x^2-1\right)\frac{d\widetilde{R}_\nu}{dx}\right] + \left[-\frac{(\nu+1)^2}{x^2-1} - \nu(\nu+1)\right]\widetilde{R}_\nu = 0. \tag{113}$$

This is Eq. (92), with $\nu(\nu+1)$ replacing the angular effective mass and with the fundamental frequency given above. For every $\nu > 0$, Eq. (112) exhibits the horizon-ingoing behavior $(x-1)^{-(\nu+1)/2}$ and the decaying outer behavior $x^{-\nu-1}$. The radial normalization remains finite and nonzero throughout this auxiliary family. We may therefore take the limit directly and obtain

$$R_{00}(x) = \lim_{\nu\to 0^+}\widetilde{R}_\nu(x) = \frac{1}{\sqrt{x^2-1}}. \tag{114}$$

The limiting function is nonzero and satisfies the $\ell = 0$ throat equation at

$$\widehat{\omega}_{00} = -i. \tag{115}$$

Indeed,

$$\frac{d}{dx}\left[\left(x^2-1\right)\frac{dR_{00}}{dx}\right] - \frac{R_{00}}{x^2-1} = 0. \tag{116}$$

Its endpoint behavior is

$$R_{00}(x) = \frac{1}{\sqrt{2}}(x-1)^{-1/2}\left[1 - \frac{x-1}{4} + O\left((x-1)^2\right)\right] \tag{117}$$

near the event horizon, while

$$R_{00}(x) = \frac{1}{x} + \frac{1}{2x^3} + O\left(x^{-5}\right) \tag{118}$$

at the outer end of the throat. The former has the required ingoing exponent $-i\widehat{\omega}_{00}/2 = -1/2$, whereas the latter contains only the decaying large-x branch. Thus, the fundamental frequency is a nontrivial quasinormal resonance. The apparent zero obtained by setting $\nu = 0$ before fixing the normalization is removable.

Restoring dimensions gives

$$\omega_{00}^{\mathrm{NE}} = -i\kappa_{\mathrm{NH}} + O(\eta^2). \tag{119}$$

The leading dimensionless frequency contains no factor of v_1/v_2. Therefore, no first-order term proportional to either four-derivative coefficient survives in $-\mathrm{Im}\,\omega_{00}^{\mathrm{NE}}/\kappa_{\mathrm{NH}}$. Combined with Eq. (89), this yields

$$\beta_{00}^{\mathrm{NE}} = 1 + O(\eta) + O(\varepsilon\eta) + O(\varepsilon^2), \tag{120}$$

and therefore

$$\lim_{\eta\to 0}\beta_{00}^{\mathrm{NE}} = 1 + O(\varepsilon^2). \tag{121}$$

The cancellation is specific to the strictly cold endpoint. It does not constrain the finite-separation decay rate once the two black hole surface gravities differ or another quasinormal family supplies the spectral gap. The massless scalar field also admits a stationary constant solution with $\omega = 0$. We exclude this solution when defining the decay spectral gap because it does not describe a decaying perturbation.

The dominant endpoint for the neutral scalar is therefore unchanged to first order in the parity-even four-derivative interactions. This result is not inferred from a formal zero of a gamma function. It follows from the nonzero normalized radial solution in Eq. (114) and from the equality of the two black hole surface gravities at leading cold order.

$$1 > \frac{1}{2}, \tag{122}$$

The four-derivative terms considered here cannot shift the exact cold-limit endpoint across the Christodoulou threshold at first order in perturbation theory. Any displacement of the physical $\beta = 1/2$ boundary must arise at finite horizon separation.

Terms of relative order $O(\eta)$ distinguish κ_+ from κ_-, modify the near-extremal frequency in the spherically symmetric sector, and allow other quasinormal-mode families to compete with the throat family. These effects depend on more than the local extremal geometry and cannot be inferred from Eq. (110) alone.

The cold-limit calculation therefore fixes the first-order endpoint value for the dominant neutral scalar mode, whereas higher angular sectors respond to the coefficient direction C_A. The neutral-scalar Christodoulou boundary away from exact extremality must probe additional information contained in the full charged de Sitter exterior.

CPC Accepted

IV. FULL EXTERIOR SPECTRUM AND FAMILY COMPETITION

A. Finite-distance quasinormal problem

The cold-limit analysis isolates the local throat spectrum but cannot determine the finite-distance neutral-scalar Christodoulou boundary. We therefore solve the scalar quasinormal-mode problem on the fully corrected exterior geometry while holding fixed the geometric distance from cold extremality. This choice is essential because the four-derivative interactions shift the extremal charge and mass themselves.

1. *Finite-distance parametrization*

We specify the two black-hole horizons by

$$r_- = r_e(1-\eta), \qquad r_+ = r_e(1+\eta), \qquad 0<\eta<1. \tag{123}$$

We keep r_e, $z=\Lambda r_e^2$, and η fixed while varying c_1 and c_3. The mass and electric charge must therefore vary so that both radii in Eq. (123) remain roots of the corrected metric.

We expand

$$M = M_0 + \varepsilon M_1 + O(\varepsilon^2), \qquad Q^2 = Q_0^2 + \varepsilon Q_1^2 + O(\varepsilon^2). \tag{124}$$

At the two-derivative order, the two horizon conditions yield

$$M_0 = r_e\left[1-\frac{2z(1+\eta^2)}{3}\right], \tag{125}$$

and

$$Q_0^2 = \frac{4r_e^2}{3}(1-\eta^2)\left[3-(3+\eta^2)z\right]. \tag{126}$$

It is useful to introduce

$$\mathcal{A}(z,\eta) = 3(1-z)-\eta^2 z. \tag{127}$$

Expanding $f(r_\pm)=0$ to first order yields two linear equations for M_1 and Q_1^2. We obtain

$$M_1 = \frac{2\mathcal{A}}{45r_e(1-\eta^2)^2}\mathcal{M}(z,\eta), \tag{128}$$

where

$$\mathcal{M}(z,\eta) = 32c_1(1+\eta^2)\mathcal{A} + c_3\left[21-9\eta^2-6z-8\eta^2 z-2\eta^4 z\right]. \tag{129}$$

The charge shift is

$$Q_1^2 = \frac{32\mathcal{A}}{45(1-\eta^2)^2}\mathcal{Q}(z,\eta), \tag{130}$$

with

$$\mathcal{Q}(z,\eta) = 4c_1\left(5+10\eta^2+\eta^4\right)\mathcal{A} + c_3\left[15-3\eta^4-20\eta^2 z+8\eta^4 z-4\eta^6 z\right]. \tag{131}$$

These expressions smoothly reduce to the corrected cold relations as $\eta\to 0$. In particular,

$$\lim_{\eta\to 0} M_1 = \frac{2(1-z)}{5r_e}\left[32c_1(1-z)+c_3(7-2z)\right], \tag{132}$$

and

$$\lim_{\eta\to 0} Q_1^2 = 32(1-z)\left[c_3+4c_1(1-z)\right]. \tag{133}$$

Thus, the finite-distance family connects continuously to the corrected cold branch.

Once M and Q are fixed, the cosmological horizon r_c is obtained as the largest positive root of the corrected radial function. We determine r_c perturbatively or numerically from

$$f(r_c)=0, \qquad r_c > r_+. \tag{134}$$

We use the resulting root to evaluate κ_c and impose the outer boundary condition.

2. *Regular radial field*

The scalar equation derived previously can be expressed directly in terms of the areal-radius coordinate by defining

$$P(r) = e^{\psi(r)} f(r). \tag{135}$$

It then takes the form

$$P^2\Psi'' + PP'\Psi' + \left(\omega^2 - V_\ell\right)\Psi = 0. \tag{136}$$

The quasinormal behavior at the two outer horizons is known analytically; therefore, we factor it out before discretizing the radial equation.

$$\Psi(r) = e^{\omega S(r)} y(r), \tag{137}$$

CPC Accepted

where

$$S(r) = -\frac{i}{2\kappa_+}\ln(r-r_+) - \frac{i}{2\kappa_c}\ln(r_c-r). \tag{138}$$

The remaining function $y(r)$ is regular over the closed interval $r_+ \leqslant r \leqslant r_c$.

Substituting Eq. (137) into Eq. (136) and dividing by P yields

$$\left[\mathcal{L}_0 + \omega\mathcal{L}_1 + \omega^2\mathcal{L}_2\right] y = 0. \tag{139}$$

The frequency-independent operator is

$$\mathcal{L}_0 y = Py'' + P'y' - \frac{V_\ell}{P}y. \tag{140}$$

The term linear in frequency is

$$\mathcal{L}_1 y = 2PS'y' + (PS'' + P'S')y, \tag{141}$$

while the quadratic term is

$$\mathcal{L}_2 y = \left[P(S')^2 + \frac{1}{P}\right] y. \tag{142}$$

The apparent singularities in Eqs. (140)–(142) cancel when the exact horizon powers in Eq. (138) are included. The resulting equation is regular at both endpoints.

3. *Endpoint equations*

We impose the regular horizon limits analytically rather than numerically evaluating expressions that contain differences of singular terms.

Let r_h denote either r_+ or r_c, and write

$$q_h = P'(r_h), \qquad s_h = -\frac{i}{2\kappa_h}. \tag{143}$$

Near the chosen horizon,

$$S' = \frac{s_h}{r-r_h} + S_h^{\rm reg} + O(r-r_h), \tag{144}$$

where $S_h^{\rm reg}$ denotes the finite contribution from the opposite horizon factor.

$$s_h^2 = -\frac{1}{q_h^2}, \tag{145}$$

The leading pole in $\mathcal{L}_2$ cancels exactly.

We also define the finite-horizon value

$$W_h = \left.\frac{V_\ell}{P}\right|_{r=r_h}. \tag{146}$$

Taking the limit in Eq. (139) yields the regular endpoint equation.

$$\begin{aligned} 0 = {} & \left[q_h + 2\omega q_h s_h\right] y'(r_h) \\ & + \left[-W_h + \omega\left(q_h S_h^{\rm reg} + \frac{P''(r_h)s_h}{2}\right)\right. \\ & \left. + \omega^2\left(2q_h s_h S_h^{\rm reg} - \frac{P''(r_h)}{q_h^2}\right)\right] y(r_h). \end{aligned} \tag{147}$$

We obtained Eq. (147) by expanding the three operators near a simple horizon, where the divergent terms cancel.

The finite quantities appearing in Eq. (144) take a particularly simple form,

$$S_+^{\rm reg} = \frac{i}{2\kappa_c(r_c-r_+)}, \tag{148}$$

and

$$S_c^{\rm reg} = -\frac{i}{2\kappa_+(r_c-r_+)}. \tag{149}$$

Thus, Eq. (147) provides both endpoint rows of the spectral problem without introducing an auxiliary boundary condition.

4. *Chebyshev discretization*

We map the exterior interval to

$$-1 \leqslant \xi \leqslant 1 \tag{150}$$

through

$$r(\xi) = \frac{r_c+r_+}{2} + \frac{r_c-r_+}{2}\xi. \tag{151}$$

For the pseudospectral discretization, we use the standard Chebyshev–Lobatto grid [61],

$$\xi_j = \cos\left(\frac{j\pi}{N}\right), \qquad j = 0,\ldots,N. \tag{152}$$

Following the linear coordinate transformation, the first and second radial derivatives are represented by finite matrices. Evaluating Eqs. (140)–(142) at these nodes

CPC Accepted

yields three matrices, L_0, L_1, and L_2. We replace their endpoint rows with those specified by Eq. (147).

The resulting quadratic spectral equation takes the standard quadratic-eigenvalue form [62],

$$\left(L_0+\omega L_1+\omega^2 L_2\right)\mathbf{y}=0. \tag{153}$$

We use the standard companion linearization of this quadratic eigenvalue problem and introduce

$$\mathbf{u}=\begin{pmatrix}\mathbf{y}\\ \omega\mathbf{y}\end{pmatrix}. \tag{154}$$

The quasinormal frequencies then satisfy

$$\begin{pmatrix}0 & I\\ -L_0 & -L_1\end{pmatrix}\mathbf{u}=\omega\begin{pmatrix}I & 0\\ 0 & L_2\end{pmatrix}\mathbf{u}. \tag{155}$$

This formulation enables us to obtain multiple frequencies at fixed (z,η,ℓ,c_1,c_3) from a single spectral solve.

5. *Mode identification and convergence*

We retain only eigenvalues that remain stable as the Chebyshev order increases, have regular reduced radial profiles, and vary continuously under small changes in z, η, and the effective coefficients. Near cold extremality, the $\ell\geqslant 1$ purely damped branches must approach Eq. (110), while the fundamental $\ell=0$ branch must approach Eq. (119). The oscillatory large-ℓ branch must approach the null-orbit result derived below. We make the numerical selection explicit by computing each candidate spectrum at $N=40$, 60, and 80. For each candidate eigenvalue ω_N, we define the inter-order drift as $\Delta_{N,N'}=|r_e\omega_N-r_e\omega_{N'}|/(1+|r_e\omega_N|)$. We also evaluate the normalized generalized-eigenvalue residual $\rho_N=\|A_N\mathbf{u}-\omega_N B_N\mathbf{u}\|_2/[(\|A_N\|_2+|\omega_N|\|B_N\|_2)\|\mathbf{u}\|_2]$, where A_N and B_N are the corresponding companion matrices. We accept a candidate only if $\max(\Delta_{40,60},\Delta_{60,80})<10^{-7}$ and $\rho_N<10^{-10}$ for all three orders. After normalizing the reduced radial vector by $\max_j|y_j|=1$, we also require finite endpoint values and no new grid-scale oscillations as N is increased. These requirements are applied before the spectral infimum is formed.

For fixed ℓ, we follow an accepted mode across parameter space by selecting the accepted eigenvalue closest in the complex-frequency plane to the preceding point. In regions where two accepted branches approach one another, we repeat the continuation from both directions and retain the separate branches. Family labels are then assigned according to independent limiting behavior. The purely damped near-extremal family approaches the analytic cold spectrum, the oscillatory high-angular family approaches the null-orbit expression, and the de Sitter-type family approaches the pure-de Sitter frequencies given below. The finite-angular cascade discussed later is simpler because each competing branch has a distinct value of ℓ.

Three representative convergence sequences are shown below. The frequencies are reported as $r_e\omega$. For an oscillatory conjugate pair, we list the member with positive real part.

Table 1 presents representative cases from the near-extremal, photon-sphere, and finite-ℓ regimes used in the family comparison. The largest visible change between successive orders occurs for the near-cold $\ell=0$ example between $N=40$ and 60, whereas the $N=60$ and 80 values agree to substantially higher precision. The two oscillatory examples exhibit the same convergence pattern and remain comfortably within the acceptance thresholds.

We identify the de Sitter–type family independently by decreasing r_e at fixed Λ and fixed η, with $z=\Lambda r_e^2$. Along this path, $M,Q\to 0$, and the exterior approaches the static de Sitter patch. The slower nonstationary scalar branch, which is the branch relevant to the spectral infimum, tends to the pure de Sitter form [23],

$$\omega_{n\ell}^{\mathrm{dS}}=-i\sqrt{\frac{\Lambda}{3}}(\ell+2n),\qquad n=0,1,2,\ldots, \tag{156}$$

with the $\ell=n=0$ constant solution excluded from the decay rate. The second pure de Sitter scalar branch is more strongly damped and therefore does not affect the spectral-infimum comparison considered here. We continuously follow the fundamental nonstationary $\ell=1$ member back to the black hole of interest. This procedure separates the outer family from purely imaginary near-extremal resonances and completes the family identification required to determine the spectral gap.

B. Mode-family transitions

The physical origin of the spectral gap changes along the charged de Sitter family. Near cold extremality, the purely damped throat mode is the slowest, whereas at larger normalized horizon separation, an oscillatory photon-sphere family becomes dominant. At larger z, finite angular momentum alters the ordering before the formal eikonal limit is reached. Because the gap is the lower envelope of the individual quasinormal branches, a change in the minimizing branch can also produce a kink in the parameter dependence of the gap, even though each individual branch varies smoothly.

1. *Near-extremal and photon-sphere families*

The cold-limit analysis directly yields the purely damped family. For the spherically symmetric funda-

CPC Accepted

Table 1. Representative convergence with Chebyshev order for accepted quasinormal modes. The residual column reports the conservative upper bound over $N = 40, 60, 80$.

case	$N = 40$	$N = 60$	$N = 80$	$\max \rho_N$
$z = 0.10,\ \eta = 0.05,\ \ell = 0$	$-0.04000840893i$	$-0.04000839127i$	$-0.04000839125i$	$< 10^{-11}$
$z = 0.10,\ \eta = 0.13,\ \ell = 4$	$0.8953219855 - 0.06894974113i$	$0.8953219820 - 0.06894973933i$	$0.8953219820 - 0.06894973932i$	$< 10^{-11}$
$z = 0.40,\ \eta = 0.06300965,\ \ell = 1$	$0.05453564884 - 0.008344811393i$	$0.05453564891 - 0.008344811469i$	$0.05453564899 - 0.008344811498i$	$< 10^{-11}$

mental mode, Eq. (119) gives the strict cold-limit behavior. At $z = 0.1$ and $\eta = 0.05$, we find $\kappa_- r_e = 0.04468144$, $\omega_{00} r_e \simeq -0.0400085i$, and $\beta_{00} \simeq 0.895$, consistent with the approach to $\beta = 1$. The near-extremal dominance follows from the scale separation produced by the nearly degenerate horizons. The throat modes inherit a damping scale set by the small near-horizon surface gravity, so their decay becomes slow as $\eta \to 0$. The photon-sphere and de Sitter-type families do not exhibit the same cold-limit suppression. The spectral gap is therefore determined by the throat family sufficiently close to the cold endpoint.

For the oscillatory family, we use the standard null-geodesic/eikonal correspondence [42] and define

$$A(r) = e^{2\psi(r)} f(r), \quad U(r) = \frac{A(r)}{r^2},$$
$$U'(r_{\rm ph}) = 0, \quad U''(r_{\rm ph}) < 0. \tag{157}$$

The orbital frequency and Lyapunov exponent are

$$\Omega_{\rm ph} = \frac{\sqrt{A(r_{\rm ph})}}{r_{\rm ph}}, \qquad \lambda_{\rm ph}^2 = -\frac{r_{\rm ph}^2 f(r_{\rm ph})}{2} U''(r_{\rm ph}). \tag{158}$$

At large ℓ,

$$\omega_\ell^{\rm ph} = \ell \Omega_{\rm ph} - \frac{i}{2}\lambda_{\rm ph} + O(\ell^0), \qquad \beta_{\rm ph} = \frac{\lambda_{\rm ph}}{2\kappa_-} + O(\ell^{-1}). \tag{159}$$

This family depends on the exterior null orbit and therefore probes information not contained in the local extremal throat. As the horizon separation increases, the cold suppression of throat damping weakens, whereas the photon-sphere damping remains tied to the instability timescale of the outer unstable null orbit. The oscillatory family can then lie below the throat family. For larger z, finite-wavelength corrections to the eikonal sequence become sufficiently large to alter the angular ordering that determines the infimum. Our numerical spectrum establishes this ordering directly and shows that the minimum passes through a short sequence of finite ℓ values.

2. *Transition and complete scalar gap*

At $z = 0.1$ and $\eta = 0.13$, the finite-angular ratios $\beta_{\ell=1,2,3,4} \simeq 0.51160, 0.49713, 0.49336, 0.49182$ already indicate the transition from the near-extremal branch to the photon-sphere sector. At the eikonal threshold, finite-angular modes approach one-half from above for $z = 0.2$ and $z = 0.3$. The corresponding values for $\ell = 1, 2, 3, 4$ are $(0.51411, 0.50465, 0.50232, 0.50139)$ and $(0.50265, 0.50084, 0.50042, 0.50025)$. At $z = 0.4$, the ordering is reversed. At the eikonal threshold, we obtain $\beta_{\ell=1,2,3} \simeq 0.49830, 0.49942, 0.49971$; thus, the finite $\ell = 1$ mode crosses first.

A denser sweep localizes the onset of this finite-angular reordering.

$$0.3365 < z < 0.3370. \tag{160}$$

Figure 1 shows the sign change of the finite-angular excess relative to one half.

For the neutral scalar sector, following the Christodoulou spectral criterion for charged de Sitter black holes [19, 21], the spectral gap is defined as

$$\alpha = \inf_{\substack{n,\ell \\ \omega_{n\ell} \neq 0}} \{-\mathrm{Im}\,\omega_{n\ell}\}, \qquad \beta = \frac{\alpha}{\kappa_-}. \tag{161}$$

Here α denotes the exterior spectral gap. It is unrelated to the order-counting parameter ε used for the four-derivative expansion. The infimum is required because the photon-sphere sequence can approach its limiting damping rate without attaining it at finite ℓ. The physical meaning of the change of family is then simple. When the throat family determines α, both the decay rate in the numerator and the inner-horizon blueshift scale in the denominator inherit near-horizon physics. Once photon-sphere modes determine α, the numerator is fixed by the global exterior geometry, whereas κ_- remains a Cauchy-horizon quantity. The Christodoulou ratio then compares scales associated with different regions of the spacetime. This change permits the finite-distance response to reverse sign, even though the strict cold endpoint remains unchanged.

The lower-envelope character is important in the narrow angular-reordering region. A denser finite-angular-momentum calculation shows that the branch that reaches $\beta = 1/2$ first leaves the eikonal limit through large but finite ℓ. Representative points give $\ell = 6$ at $z = 0.3370$, $\ell = 4$ at $z = 0.3372$, $\ell = 3$ at $z = 0.3376$, and $\ell = 2$ at $z = 0.3382$. The $\ell = 2$ branch remains the first finite-angular-momentum crossing near $z = 0.339$, while $\ell = 1$ be-

CPC Accepted

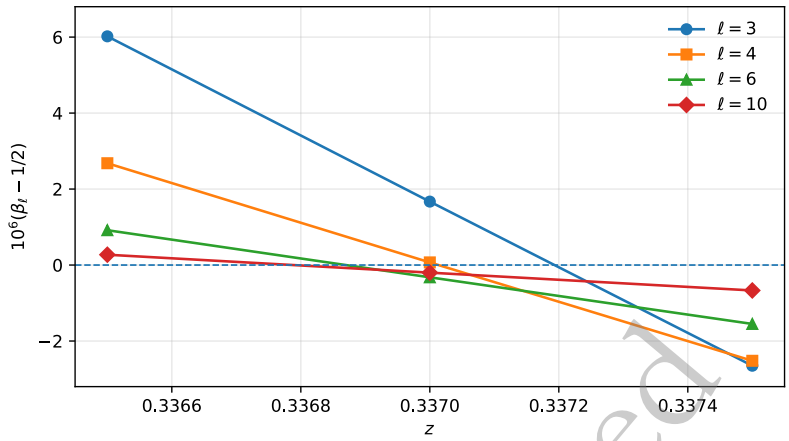

Fig. 1. Finite-angular-momentum departure from the eikonal neutral-scalar Christodoulou threshold. The plotted finite-ℓ quantity is $\beta_\ell - 1/2$, evaluated at the two-derivative eikonal crossing for each z. Negative values indicate that the corresponding finite-ℓ mode reaches the threshold before the eikonal sequence. The first sign change occurs between $z = 0.3365$ and $z = 0.3370$. Beyond this onset, the photon-sphere mode that minimizes the threshold passes through successively lower angular sectors and is carried by the $\ell = 1$ sector at $z = 0.3400$.

comes the minimizing branch by $z = 0.3400$. The ordering is unchanged when the representative comparisons are repeated at spectral orders $N = 40, 50, 60$. Thus, the transition is a short cascade of finite-angular-momentum branches rather than a direct differentiable continuation from $\ell \to \infty$ to $\ell = 1$.

Table 2 summarizes the parts of the (z, η) plane that are directly fixed by the calculations above. It is intentionally restricted to the strict near-cold regime and to the two-derivative Christodoulou boundary. We do not infer a complete partition of the full two-parameter plane from these samples.

We also compare the near-extremal and de Sitter-type branches at representative neutral-scalar Christodoulou crossings. The near-extremal values of the ratio at $z = 0.05, 0.10, 0.20, 0.30, 0.40$ are $0.82399, 0.82835, 0.80731, 0.67539, 0.57594$, respectively. The continued de Sitter-type branch yields $\beta_{\rm dS} \simeq 0.81401, 1.33093, 2.75$ at the first three points and remains above 4 at $z = 0.30$ and 0.40. Thus, neither family approaches the Christodoulou threshold at the crossings considered below. The eikonal photon-sphere sequence provides the infimum at the representative points through $z = 0.30$. After the narrow angular-reordering band, the finite $\ell = 1$ branch provides the infimum from $z = 0.3400$ through the larger-z points considered here, including $z = 0.40$.

V. NEUTRAL-SCALAR CHRISTODOULOU BOUNDARY AND COEFFICIENT-SPACE INTERPRETATION

A. Displacement of the neutral-scalar Christodoulou boundary

We now determine how the four-derivative interactions shift the finite-distance Christodoulou boundary. Away from an exact mode-family exchange, let j denote the unique quasinormal branch that attains the spectral infimum near the crossing. In the following equations, we suppress the branch label and understand β, b_i, and B_i as quantities associated with this active branch. At two-derivative order, we define $\eta_*^{(0)}(z)$ by

$$\beta_0\left(z, \eta_*^{(0)}\right) = \frac{1}{2}. \tag{162}$$

For fixed r_e, z, and η, write

$$\beta = \beta_0 + \frac{\varepsilon}{r_e^2}\left[b_1(z,\eta)c_1 + b_3(z,\eta)c_3\right] + O(\varepsilon^2), \tag{163}$$

and

$$\eta_*(z) = \eta_*^{(0)}(z) + \frac{\varepsilon}{r_e^2}\left[B_1(z)c_1 + B_3(z)c_3\right] + O(\varepsilon^2). \tag{164}$$

Expanding the threshold condition gives

$$B_i(z) = -\frac{b_i\left(z, \eta_*^{(0)}\right)}{\partial_\eta \beta_0\big|_*}, \qquad i \in \{1, 3\}. \tag{165}$$

The coefficient B_i therefore measures the displacement of the threshold in normalized horizon separation. It is distinct from the fixed-geometry correction b_i to the regularity ratio itself. This derivative exists as a standard branch derivative when the minimizing mode is unique. For the monotonic threshold crossings considered here, at an exact exchange between two branches a and b, the physical threshold is the lower envelope $\eta_* = \min(\eta_*^{(a)}, \eta_*^{(b)})$. If their response vectors differ,

CPC Accepted

Table 2. Representative sources of the neutral-scalar spectral gap in the regions identified directly in this work. Entries on the Christodoulou boundary refer to $\eta = \eta_*^{(0)}(z)$. The eikonal entry denotes the large-ℓ photon-sphere sequence. The angular-reordering band contains the finite-ℓ cascade described in the text.

region	location	family supplying the gap
near-cold	$\eta \to 0$	near-extremal throat, $\ell = 0$
small and intermediate z boundary	$z = 0.05, 0.10, 0.20, 0.30$	eikonal photon sphere
reordering onset	$0.3365 < z < 0.3370$	eikonal to finite ℓ
finite-angular cascade	$0.3370 \le z < 0.3400$	finite-ℓ photon sphere
larger-z boundary	$(z, \eta) = (0.40, 0.06300965)$	$\ell = 1$ photon sphere

$\mathbf{B}^{(a)} \neq \mathbf{B}^{(b)}$, the lower envelope has no unique two-sided derivative at the exchange. Along any specified coefficient direction, one instead uses the one-sided response of the branch that gives the smaller displaced threshold. We therefore treat B_i branchwise in the transition region and do not infer a unique response vector exactly at a mode crossing. Since $r_e = (r_+ + r_-)/2$ and $\eta = (r_+ - r_-)/(r_+ + r_-)$, the sign of $\delta\eta_*$ indicates whether the threshold moves farther from or closer to the cold endpoint in normalized areal horizon separation. It does not define a volume on the full black-hole parameter space.

Table 3 summarizes the representative crossings. At $z = 0.1$, for example, $\partial_\eta \beta_0|_* = -5.01440741$, $b_1 = 30.86105181$, and $b_3 = 4.28413287$, yielding $B_1 = 6.15447635$ and $B_3 = 0.85436474$. At $z = 0.40$, the finite-$\ell = 1$ branch gives $\partial_\eta \beta_0|_* \simeq -10.2140$, $b_1 \simeq -12.5563$, and $b_3 \simeq -4.18944$. Using symmetric coefficient steps between 10^{-4} and 2.5×10^{-5} in c_i/r_e^2 changes the final B_i values by less than 10^{-5}, while variation in the Chebyshev order gives the conservative uncertainties quoted in the table.

Positive c_1 or c_3 therefore shifts the threshold to larger η at small and intermediate z, but toward the cold endpoint at larger z. The response must be interpreted branch-wise across the narrow family-exchange region and need not be differentiable at the exact exchange points. Once the $\ell = 1$ branch becomes the unique minimizer by $z = 0.3400$, its response components vary smoothly and yield

$$z_{B_3} = 0.34497, \qquad z_{B_1} = 0.36870. \tag{166}$$

These zeros are not located within the ambiguous exchange band. At $z = 0.34497$, the two-derivative crossing occurs at $\eta_*^{(\ell=1)} = 0.08431487$, whereas the $\ell = 2$ and eikonal crossings occur at 0.08433719 and 0.08435291, respectively. At $z = 0.36870$, the corresponding values are 0.07592823, 0.07601924, and 0.07606750. Thus, the $\ell = 1$ branch uniquely attains the spectral infimum at both zeros. Repeating the coefficient-step and spectral-order tests leaves the rounded values $z_{B_3} = 0.34497$ and $z_{B_1} = 0.36870$ unchanged. Figure 2 displays the eikonal and $\ell = 1$ branch responses on either side of the narrow exchange region.

The sign reversal is consistent with the unchanged cold endpoint established by the normalized $\ell = 0$ solution. The dominant throat mode satisfies $\delta\beta_{00}|_{\eta=0} = 0$ to first order, whereas B_i measures a finite-η crossing that depends on the relevant exterior scalar spectrum and unequal horizon surface gravities. Away from exact branch exchanges and at fixed z, the first-order threshold remains unchanged.

$$B_1(z)c_1 + B_3(z)c_3 = 0. \tag{167}$$

Therefore, no single combination of coefficients determines the boundary motion throughout the cold branch.

Table 3. Two-derivative neutral-scalar Christodoulou crossings and first-order branch responses are defined by Eq. (164). A positive B_i shifts the threshold to larger η for positive c_i, whereas a negative B_i shifts it toward the cold endpoint. The first four rows lie in the eikonal photon-sphere region, and the last row lies in the finite-$\ell = 1$ region. None of the tabulated points corresponds to an exact mode-family exchange.

z	$\eta_*^{(0)}$	$B_1(z)$	$B_3(z)$	spectral family
0.05	0.13166844	6.82389	0.93384	$\ell \to \infty$
0.10	0.12787994	6.15448	0.85436	$\ell \to \infty$
0.20	0.11656132	4.50290	0.63001	$\ell \to \infty$
0.30	0.09723997	2.20645	0.25718	$\ell \to \infty$
0.40	0.06300965	−1.2293(1)	−0.41016(3)	$\ell = 1$

B. Effective coefficient plane

The preceding results define three linear response relations in the (c_1, c_3) plane. Using Eqs. (31), (41), and (164), we write

$$\begin{aligned} C_M(z) &= 8(1-z)c_1 + (3+2z)c_3, \\ C_A(z) &= 8(1-z)c_1 + c_3, \\ C_\beta(z) &= B_1(z)c_1 + B_3(z)c_3. \end{aligned} \tag{168}$$

CPC Accepted

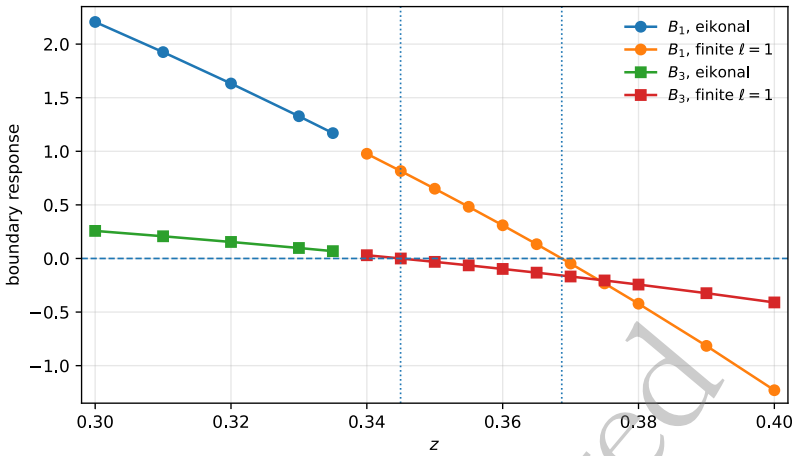

Fig. 2. Branchwise finite-distance neutral-scalar boundary response. The plotted functions are $B_1(z)$ and $B_3(z)$ from Eq. (164). For a positive coefficient, positive values shift the threshold to larger normalized horizon separation, whereas negative values shift it toward the cold endpoint. The eikonal and finite $\ell = 1$ branches are shown explicitly. Intermediate finite-angular-momentum branches provide the lower envelope in the narrow family-exchange band, where the spectral gap need not have a single derivative. The dotted lines mark $z_{B_3} = 0.34497$ and $z_{B_1} = 0.36870$, both in the region where $\ell = 1$ uniquely supplies the gap.

These quantities govern different derivatives. The first fixes the fixed-charge extremal mass-parameter shift; the second fixes the local throat deformation and the higher-angular-momentum cold spectrum; and the third fixes the finite-distance displacement $\delta\eta_* = (\varepsilon/r_e^2)C_\beta$. The form C_β is branch-dependent whenever the spectral infimum changes family. It is well defined as a single linear form when one branch uniquely determines the gap, including the two zero locations quoted above. However, no unique C_β exists at an exact branch exchange if the competing branch responses differ. Their zero lines therefore compare inequivalent physical responses in a common coefficient space.

The analytic zero-line slopes are

$$\left.\frac{c_3}{c_1}\right|_{C_M=0} = -\frac{8(1-z)}{3+2z}, \qquad \left.\frac{c_3}{c_1}\right|_{C_A=0} = -8(1-z),$$
$$\left.\frac{c_3}{c_1}\right|_{C_\beta=0} = -\frac{B_1}{B_3}, \tag{169}$$

when $B_3 \neq 0$. The first two are distinct because $C_M - C_A = 2(1+z)c_3$, whereas the third is determined only after solving the exterior spectral problem.

At $z = 0.1$, the three slopes are approximately -2.25, -7.2, and -7.20357 for C_M, C_A, and C_β, respectively. The near coincidence of the latter two is incidental because they are obtained from different calculations. At $z = 0.4$, the slopes become -1.26316, -4.8, and -2.99716. In addition, **B** has reversed orientation, so positive c_1 and positive c_3 yield $C_\beta < 0$ there.

The sign structure makes the physical inequivalence explicit. Along a ray with $C_M > 0$, the extremal mass parameter decreases, while the same ray can have either sign of C_β as z changes. For $\ell \geqslant 1$, the strict cold spectral correction instead has the sign of C_A. A single coefficient ray can therefore decrease the extremal mass parameter, increase the cold value of β for higher angular modes, and still move the finite-distance threshold toward the cold endpoint. Figure 2 shows the change in the branch responses with cosmological scale. The physical lower envelope passes through the finite-angular cascade described in Section 4.2, so we do not interpret the plotted eikonal and $\ell = 1$ curves as a single differentiable response through the exchange band.

Thus, no universal four-derivative direction governs all observables considered here. Extremality probes the cold charge-energy relation, the throat probes local geometry, and the neutral-scalar boundary response combines exterior decay with Cauchy-horizon amplification.

C. Extremality and quantum-gravity interpretation

The fixed-charge cold-extremal mass-parameter shift derived in Eq. (32) has the opposite sign to C_M. Thus, $C_M > 0$ decreases the extremal mass parameter throughout the ordinary cold branch. In the asymptotically flat limit, the same direction becomes $C_M(0) = 8c_1 + 3c_3$, where the $1/r$ coefficient has its usual mass interpretation. At finite positive Λ, we use the more cautious term ``mass parameter'' because de Sitter spacetime has no unique analogue of the asymptotically flat ADM mass.

Away from an exact mode-family exchange, the neutral-scalar boundary response is governed instead by the branchwise form C_β. This distinction can be observed without tuning the coefficient ray. Along $c_1 > 0$, $c_3 = 0$, the extremal mass parameter decreases for every $0 \leqslant z < 1/2$, whereas $\delta\eta_*$ changes from $+6.15448\,\varepsilon c_1/r_e^2$ at $z = 0.1$ to $-1.2293\,\varepsilon c_1/r_e^2$ at $z = 0.4$. Along $c_1 = 0$, $c_3 > 0$, the corresponding shifts are $+0.85436\,\varepsilon c_3/r_e^2$ and $-0.41016\,\varepsilon c_3/r_e^2$. Therefore

CPC Accepted

$$\delta M_{\rm ext}|_Q < 0 \quad \not\Longrightarrow \quad \mathrm{sgn}(\delta\eta_*). \tag{170}$$

The failure follows from the quantities measured by these derivatives. The mass-parameter shift compares neighboring degenerate solutions at fixed charge, whereas the neutral-scalar Christodoulou boundary compares the full exterior spectral infimum with the inner-horizon blueshift scale. The local throat introduces a third direction, C_A. The three forms can coincide accidentally at isolated points, but they are generically inequivalent.

The weak-gravity comparison is therefore conditional. If an independently specified ultraviolet criterion and a chosen de Sitter mass prescription select coefficient directions corresponding to $C_M > 0$, our result determines the motion of the neutral-scalar Christodoulou threshold only after their location relative to the z-dependent line $C_\beta = 0$ is known. At smaller z, regions with $C_M > 0$ can also have $C_\beta > 0$. At larger z, the same extremality sign can coexist with $C_\beta < 0$. Extremality alone therefore cannot predict the fate of the neutral-scalar Cauchy-horizon regularity threshold.

Positive Λ is essential to this conclusion. It changes the cold throat ratio, introduces the cosmological horizon as the outer boundary of the wave problem, and reorganizes the competing quasinormal families. The local curvature-Maxwell contribution survives as $\Lambda \to 0$, but the finite-distance sign reversal depends on the global de Sitter exterior and would be absent from a calculation confined to the asymptotically flat limit.

We do not make the stronger claim that a unique de Sitter weak-gravity principle imposes a definite inequality on (c_1, c_3). Different de Sitter extremal limits and mass prescriptions require additional assumptions. Instead, our result provides the infrared map from any independently selected coefficient region to the direction in which the linear neutral-scalar Christodoulou threshold moves.

VI. VALIDITY AND SCOPE

A. Perturbative domain and limits

The four-derivative coefficients have dimensions of length squared; therefore, we define

$$\lambda_4 = \frac{\varepsilon}{r_e^2}\max(|c_1|,|c_3|), \qquad \lambda_4 \ll 1. \tag{171}$$

For the ordinary cold branch $0 \leqslant z < 1/2$, this constitutes a conservative local effective-theory condition. The cold throat imposes the stronger requirement

$$\left|\frac{8\varepsilon(1-z)}{r_e^2(1-2z)}C_A(z)\right| \ll 1, \tag{172}$$

or without relying on coefficient cancellations,

$$\frac{\varepsilon\max(|c_1|,|c_3|)}{r_e^2(1-2z)} \ll 1. \tag{173}$$

The immediate ultracold neighborhood therefore requires a separate scaling analysis.

The near-extremality parameter η is independent of the local effective expansion. If two nearly coincident simple roots are perturbed at fixed two-derivative values of M and Q, Eq. (45) gives $|\delta r_\pm|/r_e = O(\lambda_4/\eta)$. Thus, this particular expansion requires $\lambda_4 \ll \eta^2$. Our finite-distance parametrization instead fixes r_- and r_+ geometrically and solves for M and Q, which removes this artificial hierarchy. The analytic throat calculation retains the leading η and $\varepsilon\eta$ terms, whereas the finite-distance neutral-scalar Christodoulou boundary follows from the full exterior scalar problem.

The limits $\eta \to 0$ and $\varepsilon \to 0$ commute for the strict first-order value of the fundamental scalar endpoint because Eqs. (119) and (120) contain no $O(\varepsilon)$ term independent of η. The $\Lambda \to 0$ limit is different. Local quantities have smooth limits, but the cosmological horizon moves to infinity and the global de Sitter quasinormal-mode problem changes character. We therefore do not interpret the $z \to 0$ continuation of the finite-distance threshold as an asymptotically flat neutral-scalar Christodoulou boundary.

B. Normalization, field variables, and spectral reliability

A constant rescaling of time, $t' = e^C t$, implies $\omega' = e^{-C}\omega$ and $\kappa'_a = e^{-C}\kappa_a$. Hence,

$$\frac{-\mathrm{Im}\,\omega'}{\kappa'_-} = \frac{-\mathrm{Im}\,\omega}{\kappa_-}, \tag{174}$$

Thus, the regularity ratio is independent of the additive normalization of ψ.

The field-variable convention was fixed by the reduced action in Section 2. We assign no frame-independent meaning to c_1 or c_3 separately. Instead, the calculation refers to the explicitly specified gravitational action together with the minimally coupled neutral scalar. A consistent field redefinition across all sectors yields an equivalent description order by order, whereas changing the gravitational variables and then imposing a new minimal scalar coupling would define a different spectator theory.

The spectral gap is established by comparing the near-extremal, de Sitter-type, finite-angular photon-sphere, and eikonal families, rather than by tracking a single branch. The representative sequences satisfy the inter-order acceptance condition stated above. For the three cases in Table 1, the $N = 60$ and 80 values differ at the 10^{-10} level or better, and the normalized generalized-

CPC Accepted

eigenvalue residuals remain below 10^{-11}. The fine angular sweep localizes the first deviation from the eikonal ordering to $0.3365 < z < 0.3370$. Repeating the branch comparison at $N = 40, 50, 60$ gives the same finite-angular sequence near representative points, with $\ell = 6$ at $z = 0.3370$, $\ell = 4$ at 0.3372, $\ell = 3$ at 0.3376, $\ell = 2$ at 0.3382, and $\ell = 1$ by 0.3400. Exact exchanges between consecutive branches are treated as lower-envelope kinks rather than as points with a unique derivative. Symmetric coefficient steps from 10^{-4} to 2.5×10^{-5} in c_i/r_e^2, together with the spectral-order tests, leave the zero locations $z_{B_3} = 0.34497$ and $z_{B_1} = 0.36870$ unchanged at the quoted precision. Both zeros lie well within the $\ell = 1$ region rather than at a family exchange. The acceptance thresholds and continuation procedure stated in the numerical section are used for all branches entering these comparisons. The convergence table gives representative frequencies from three distinct spectral regimes and makes the numerical precision entering the lower-envelope selection explicit.

C. Regularity criterion at the Cauchy horizon

The local Christodoulou regularity test based on the spectral ratio is standard for this problem [19, 21]. Near the Cauchy horizon, with $x = r - r_-$, the singular branch of a separated mode behaves as

$$|\Phi_s| \sim |x|^{\beta}, \qquad \beta = \frac{\alpha}{\kappa_-}. \tag{175}$$

Therefore, $|\partial_r \Phi_s|^2 \sim |x|^{2\beta-2}$, and local square integrability requires

$$\int_0^{\epsilon_0} x^{2\beta-2}\, dx < \infty \quad \Longleftrightarrow \quad \beta > \frac{1}{2}. \tag{176}$$

The case of equality is marginal and may depend on logarithmic terms. Our conclusion therefore applies to sufficiently regular linear neutral scalar perturbations. It does not establish a nonlinear theorem for the full Einstein–Maxwell effective theory, and coupled gravitational or electromagnetic sectors may alter the Cauchy-horizon behavior.

VII. CONCLUSIONS

We have studied the leading parity-even four-derivative corrections to the linear neutral-scalar Christodoulou regularity problem for charged de Sitter black holes. The analysis separates the cold extremality relation, the local extremal throat, and the finite-distance competition between exterior decay and Cauchy-horizon blueshift. These three questions probe different coefficient directions.

At the cold endpoint, the scalar problem reduces to the finite-temperature $AdS_2 \times S^2$ throat. The $\ell = 0$ associated Legendre normalization becomes singular at the fundamental resonance, but the normalized limit yields the nonzero mode $R_{00} = (x^2-1)^{-1/2}$ with $\widehat{\omega}_{00} = -i$. The common near-horizon time scale then cancels in the regularity ratio, so the dominant nonstationary spherically symmetric mode retains $\beta = 1$ to first order. Higher angular sectors still respond to the corrected throat through C_A. Thus, the absence of a first-order shift in the fundamental endpoint does not imply the absence of effective-theory corrections to the near-extremal spectrum.

The finite-distance neutral-scalar Christodoulou boundary behaves differently because the relevant exterior scalar spectrum enters. The photon-sphere family replaces the throat family as the source of the spectral gap, and finite angular momentum becomes decisive at larger z. The first departure from the eikonal ordering occurs within $0.3365 < z < 0.3370$, after which the minimizing photon-sphere branch passes through a short sequence of decreasing angular momenta and reaches $\ell = 1$ by $z = 0.3400$. The lower envelope can therefore have kinks at the exact branch exchanges, even though each branch is smooth. Positive c_1 and c_3 move the Christodoulou threshold to larger normalized horizon separation at smaller and intermediate z, but toward the cold endpoint at larger z. The two response components change sign at $z_{B_3} = 0.34497$ and $z_{B_1} = 0.36870$. Both zeros occur where the $\ell = 1$ branch uniquely supplies the spectral gap, so the mode-crossing nondifferentiability does not alter their quoted values. We make no derivative assignment at the exact exchanges within the preceding finite-angular cascade. The sign reversal is therefore a global de Sitter spectral effect rather than a deformation of the unchanged cold endpoint.

The coefficient-plane comparison makes the main implication precise. The fixed-charge extremal mass parameter responds to C_M, the local throat responds to C_A, and the finite-distance threshold responds to the z-dependent form C_β. A coefficient direction that decreases the extremal mass parameter can move the neutral-scalar Christodoulou threshold in either direction as the cosmological scale changes. Weak-gravity-inspired restrictions on extremality therefore do not determine this neutral-scalar response without additional information about the allowed coefficient region and the de Sitter mass prescription.

These conclusions hold only where the four-derivative and ordinary cold expansions remain perturbative and only for the minimally coupled neutral spectator scalar. They do not establish strong cosmic censorship for the full Einstein-Maxwell effective theory. Coupled gravito-electromagnetic perturbations can activate c_2 and can change the spectral infimum. Future work should address those sectors, rotation, and the ultracold scaling regime, where the degenerating throat and effective corrections

CPC Accepted

must be treated together. Such extensions will determine whether the cosmological-scale dependence found here persists in the full perturbative spectrum.

R. P. would like to acknowledge networking support of the COST Action CA21106 - COSMIC WISPers in the Dark Universe: Theory, astrophysics and experiments (CosmicWISPers), the COST Action CA22113 - Fundamental challenges in theoretical physics (THEORY-CHALLENGES), the COST Action CA21136 - Addressing observational tensions in cosmology with systematics and fundamental physics (CosmoVerse), the COST Action CA23130 - Bridging high and low energies in search of quantum gravity (BridgeQG), and the COST Action CA23115 - Relativistic Quantum Information (RQI), under COST (European Cooperation in Science and Technology).

References

[1] Y. Choquet-Bruhat and R. P. Geroch, Commun. Math. Phys. **14**, 329 (1969)
[2] S. Chandrasekhar and J. B. Hartle, Proceedings of the Royal Society of London. A. Mathematical and Physical Sciences **384**, 301 (1982)
[3] E. Poisson and W. Israel, Phys. Rev. D **41**, 1796 (1990)
[4] A. Ori, Phys. Rev. Lett. **67**, 789 (1991)
[5] P. R. Brady and E. Poisson, Classical and Quantum Gravity **9**, 121 (1992)
[6] P. R. Brady, I. G. Moss, and R. C. Myers, Phys. Rev. Lett. **80**, 3432 (1998), arXiv: gr-qc/9801032
[7] M. Dafermos, Commun. Pure Appl. Math. **58**, 0445 (2005), arXiv: gr-qc/0307013
[8] M. Dafermos, Commun. Math. Phys. **332**, 729 (2014), arXiv: 1201.1797[gr-qc]
[9] A. T. Franzen, Commun. Math. Phys. **343**, 601 (2016), arXiv: 1407.7093[gr-qc]
[10] J. Luk and S.-J. Oh, Duke Math. J. **166**, 437 (2017), arXiv: 1501.04598[gr-qc]
[11] M. Dafermos and Y. Shlapentokh-Rothman, Commun. Math. Phys. **350**, 985 (2017), arXiv: 1512.08260[gr-qc]
[12] J. Luk and S.-J. Oh, Strong cosmic censorship in spherical symmetry for two-ended asymptotically flat initial data i. the interior of the black hole region, Annals of Mathematics **190**, 10.4007/annals.2019.190.1.1 (2019).
[13] M. Dafermos and J. Luk, The interior of dynamical vacuum black holes i: The c0-stability of the kerr cauchy horizon, Annals of Mathematics **202**, 10.4007/annals.2025.202.2.1 (2025).
[14] F. Mellor and I. Moss, Phys. Rev. D **41**, 403 (1990)
[15] C. M. Chambers and I. G. Moss, Class. Quant. Grav. **11**, 1035 (1994), arXiv: gr-qc/9404015
[16] P. Hintz and A. Vasy, J. Math. Phys. **58**, 081509 (2017), arXiv: 1512.08004[math.AP]
[17] P. Hintz and A. Vasy, Acta Math. **220**, 1 (2018), arXiv: 1606.04014[math.DG]
[18] P. Hintz, Non-linear stability of the Kerr-Newman-de Sitter family of charged black holes (2016), arXiv: 1612.04489 [math.AP].
[19] V. Cardoso, J. L. Costa, K. Destounis, P. Hintz, and A. Jansen, Phys. Rev. Lett. **120**, 031103 (2018), arXiv: 1711.10502[gr-qc]
[20] O. J. C. Dias, F. C. Eperon, H. S. Reall, and J. E. Santos, Phys. Rev. D **97**, 104060 (2018), arXiv: 1801.09694[gr-qc]
[21] O. J. C. Dias, H. S. Reall, and J. E. Santos, Strong cosmic censorship: taking the rough with the smooth, JHEP **10**, 001, arXiv: 1808.02895 [gr-qc].
[22] M. Dafermos and Y. Shlapentokh-Rothman, Class. Quant. Grav. **35**, 195010 (2018), arXiv: 1805.08764[gr-qc]
[23] V. Cardoso, J. L. Costa, K. Destounis, P. Hintz, and A. Jansen, Phys. Rev. D **98**, 104007 (2018), arXiv: 1808.03631[gr-qc]
[24] O. J. C. Dias, H. S. Reall, and J. E. Santos, Class. Quant. Grav. **36**, 045005 (2019), arXiv: 1808.04832[gr-qc]
[25] S. Hod, Nucl. Phys. B **941**, 636 (2019), arXiv: 1801.07261[gr-qc]
[26] Z. Zhu, S.-J. Zhang, C. E. Pellicer, B. Wang, and E. Abdalla, Stability of Reissner-Nordström black hole in de Sitter background under charged scalar perturbation, Phys. Rev. D **90**, 044042 (2014), [Addendum: Phys.Rev.D 90, 049904 (2014)], arXiv: 1405.4931 [hep-th].
[27] R. Luna, M. Zilhão, V. Cardoso, J. L. Costa, and J. Natário, Strong cosmic censorship: The nonlinear story, Phys. Rev. D **99**, 064014 (2019), [Addendum: Phys.Rev.D 103, 104043 (2021)], arXiv: 1810.00886 [gr-qc].
[28] S. Hollands, R. M. Wald, and J. Zahn, Class. Quant. Grav. **37**, 115009 (2020), arXiv: 1912.06047[gr-qc]
[29] Q. Gan, G. Guo, P. Wang, and H. Wu, Phys. Rev. D **100**, 124009 (2019), arXiv: 1907.04466[hep-th]
[30] L. Chen and J. Tan, Phys. Rev. D **110**, 064003 (2024)
[31] L. Chen and F. Li, Eur. Phys. J. C **84**, 1139 (2024)
[32] H. Liu, Z. Tang, K. Destounis, B. Wang, E. Papantonopoulos, and H. Zhang, Strong Cosmic Censorship in higher-dimensional Reissner-Nordström-de Sitter spacetime, JHEP **03**, 187, arXiv: 1902.01865 [gr-qc].
[33] H. Guo, H. Liu, X.-M. Kuang, and B. Wang, Eur. Phys. J. C **79**, 891 (2019), arXiv: 1905.09461[gr-qc]
[34] K. Destounis, R. D. B. Fontana, F. C. Mena, and E. Papantonopoulos, Strong Cosmic Censorship in Horndeski Theory, JHEP **10**, 280, arXiv: 1908.09842 [gr-qc].
[35] A. K. Mishra and S. Chakraborty, Phys. Rev. D **101**, 064041 (2020), arXiv: 1911.09855[gr-qc]
[36] Q. Gan, P. Wang, H. Wu, and H. Yang, Chin. Phys. C **45**, 025103 (2021), arXiv: 1911.10996[gr-qc]
[37] R. A. Konoplya and A. Zhidenko, (In)stability of black holes in the 4D Einstein–Gauss–Bonnet and Einstein–Lovelock gravities, Phys. Dark Univ. **30**, 100697 (2020), arXiv: 2003.12492 [gr-qc].
[38] S. Aretakis, Commun. Math. Phys. **307**, 17 (2011), arXiv: 1110.2007[gr-qc]
[39] L. J. Romans, Nucl. Phys. B **383**, 395 (1992), arXiv: hep-th/9203018
[40] A. Castro, F. Mariani, and C. Toldo, Near-extremal limits of de Sitter black holes, JHEP **07**, 131, arXiv: 2212.14356 [hep-th].
[41] E. Berti, V. Cardoso, and A. O. Starinets, Class. Quant. Grav. **26**, 163001 (2009), arXiv: 0905.2975[gr-qc]
[42] V. Cardoso, A. S. Miranda, E. Berti, H. Witek, and V. T. Zanchin, Phys. Rev. D **79**, 064016 (2009), arXiv: 0812.1806[hep-th]

CPC Accepted

[43] H. Yang, D. A. Nichols, F. Zhang, A. Zimmerman, Z. Zhang, and Y. Chen, Phys. Rev. D **86**, 104006 (2012), arXiv: 1207.4253[gr-qc]
[44] A. Zimmerman and Z. Mark, Damped and zero-damped quasinormal modes of charged, nearly extremal black holes, Phys. Rev. D **93**, 044033 (2016), [Erratum: Phys.Rev.D 93, 089905 (2016)], arXiv: 1512.02247 [gr-qc].
[45] I. Davies and H. S. Reall, Phys. Rev. D **106**, 104019 (2022), arXiv: 2112.05603[gr-qc]
[46] Y. Kats, L. Motl, and M. Padi, Higher-order corrections to mass-charge relation of extremal black holes, JHEP **12**, 068, arXiv: hep-th/0606100.
[47] W. L. Boyce and J. E. Santos, EFT corrections to charged black hole quasinormal modes, JHEP **12**, 017, arXiv: 2506.10074 [hep-th].
[48] P. Bittar, S. Fichet, and L. de Souza, Phys. Rev. D **112**, 045009 (2025), arXiv: 2404.07254[hep-th]
[49] N. Arkani-Hamed, L. Motl, A. Nicolis, and C. Vafa, The String landscape, black holes and gravity as the weakest force, JHEP **06**, 060, arXiv: hep-th/0601001.
[50] C. Cheung and G. N. Remmen, Infrared Consistency and the Weak Gravity Conjecture, JHEP **12**, 087, arXiv: 1407.7865 [hep-th].
[51] C. Cheung, J. Liu, and G. N. Remmen, Proof of the Weak Gravity Conjecture from Black Hole Entropy, JHEP **10**, 004, arXiv: 1801.08546 [hep-th].
[52] Y. Hamada, T. Noumi, and G. Shiu, Phys. Rev. Lett. **123**, 051601 (2019), arXiv: 1810.03637[hep-th]
[53] B. Bellazzini, M. Lewandowski, and J. Serra, Phys. Rev. Lett. **123**, 251103 (2019), arXiv: 1902.03250[hep-th]
[54] G. Goon and R. Penco, Phys. Rev. Lett. **124**, 101103 (2020), arXiv: 1909.05254[hep-th]
[55] S. Cremonini, C. R. T. Jones, J. T. Liu, and B. McPeak, Higher-Derivative Corrections to Entropy and the Weak Gravity Conjecture in Anti-de Sitter Space, JHEP **09**, 003, arXiv: 1912.11161 [hep-th].
[56] Q.-G. Huang, M. Li, and W. Song, Weak gravity conjecture in the asymptotical dS and AdS background, JHEP **10**, 059, arXiv: hep-th/0603127.
[57] I. Antoniadis and K. Benakli, Fortsch. Phys. **68**, 2000054 (2020), arXiv: 2006.12512[hep-th]
[58] M. Montero, T. Van Riet, and V. Venken, Festina Lente: EFT Constraints from Charged Black Hole Evaporation in de Sitter, JHEP **01**, 039, arXiv: 1910.01648 [hep-th].
[59] J. Sadeghi, M. R. Alipour, and S. Noori Gashti, Strong cosmic censorship in light of weak gravity conjecture for charged black holes, JHEP **02**, 236, arXiv: 2301.11968 [hep-th].
[60] A. Sen, Black hole entropy function and the attractor mechanism in higher derivative gravity, JHEP **09**, 038, arXiv: hep-th/0506177.
[61] L. N. Trefethen, *Spectral Methods in MATLAB* (Society for Industrial and Applied Mathematics, 2000).
[62] F. Tisseur and K. Meerbergen, SIAM Review **43**, 235 (2001)

CPC Accepted